

## Understanding the Adsorption of Quinoxaline Derivatives as Corrosion Inhibitors for Mild Steel in Acidic Medium: Experimental, Theoretical and Molecular Dynamic Simulation Studies

Lgaz H<sup>1,2</sup>, Salghi R<sup>2</sup>, Jodeh S<sup>3</sup>, Ramli Y<sup>4</sup>, Larouj M<sup>1</sup>, Toumiat K<sup>5</sup>, Quraishi MA<sup>6\*</sup>, Oudda H<sup>1</sup> and Jodeh W<sup>7</sup>

<sup>1</sup>Faculty of Science, University Ibn Tofail, Morocco

<sup>2</sup>Laboratory of Applied Chemistry and Environment, Ibn Zohr University, Morocco

<sup>3</sup>Department of Chemistry, An-Najah National University, Nablus, State of Palestine

<sup>4</sup>Medical and Pharmaceutical College, University Mohammed V, Morocco

<sup>5</sup>Department of Materials Sciences, Laghouat University, Algeria

<sup>6</sup>Department of Chemistry, Indian Institute of Technology, Uttar Pradesh, India

<sup>7</sup>Department of Human Medicine, An-Najah National University, Palestine

### Abstract

The anti-corrosive properties of (E)-3-styrylquinoxalin-2(1H)-one (STQ), (E)-1-benzyl-3-(4-methoxystyryl) quinoxalin-2(1H)-one (BMQ) and (E)-3-(2-(furan-2-yl) vinyl) quinoxalin-2(1H)-one (FVQ) were analyzed by different techniques such as: potentiodynamic polarization, electrochemical impedance spectroscopy (EIS), weight loss (WL) and molecular modeling by DFT method and Monte Carlo simulation studies. All quinoxaline derivatives showed appreciable inhibition efficiency. Among the quinoxaline derivatives studied, BMQ exhibited the best inhibition efficiency. The results from the experimental and theoretical investigations show that the order of inhibition efficiency by the quinoxaline derivatives follow the order BMQ > FVQ > STQ. The experimental results suggest that the three tested inhibitors function as mixed-type compounds and the inhibition efficiency increases with the increase in inhibitor concentration and decreased with temperature. Adsorption of the three compounds on mild steel (MS) surface obeys Langmuir's isotherm model. The theoretical study by DFT method, Monte Carlo simulation and radial distribution function (RDF) provided strong evidence that the inhibition efficiency of quinoxaline derivatives is due to their ability to adsorb strongly at the MS surfaces, which is supportive of the obtained experimental results.

**Keywords:** Monte carlo; Quinoxaline; Mild steel; Corrosion inhibition; Fukui functions; DFT

### Introduction

Mild steel is an iron-containing alloy, considered as one of important constructional materials extensively used in different applications. Generally, acid solution (especially hydrochloric acid) plays a significant role in many fields of industry such as pickling, descaling and oil well acidification, its price is generally low and more consistent [1,2]. In the few last decades the use of chemical compounds as corrosion inhibitors is considered as one of the efficient and practical methods to protect the metals surfaces against aggressive mediums such as acidic solutions [3-5]. The effectiveness of these molecules is mainly from their ability to adhere to metal surfaces [6]. The use of synthetic inhibitors also appears to be economically viable and promising because of their simplicity in application, and they're relatively cheaper. Meanwhile, the adsorption of these inhibitors produces a protective insoluble film on the MS surface, which reduces contact with the corrosive mediums and consequently the degree of metal attack [7-9]. The presence of N, O, S atoms and conjugates aromatic nucleus are responsible for their essential characteristics [10]. The quinoxaline is one of the important heterocyclic compounds; they have applications in many fields such as electroluminescent materials [11,12] and in the pharmacological industry [13,14] as well as in metallic industries [15,16], this indicates that the use of the quinoxaline derivatives as inhibitors is very interesting [17,18]. The high efficiency of these compounds against corrosion can be in their rich molecular structure, which explains the high capability of these molecules to overcome corrosion. Recently, in addition to experimental investigations, the evaluation of inhibition performance is also conducted theoretically by DFT calculation and molecular dynamic simulation studies for the understanding of some experimentally unknown properties, exploring and establishing relationships between inhibitor molecules and the

metal surface [19,20]. N.A. Al-Mobarak et al. [21] have studied the corrosion inhibition of copper in 3.5% NaCl using new pyrimidine derivatives, namely, 2-mercapto-4-(p-methoxyphenyl)-6-oxo-1,6-dihydropyrimidine-5-carbonitrile (MPD) by Monte Carlo simulation and theoretical calculation, and all quantum analysis correlated well with electrochemical investigation. In addition, Youguo Yan et al. [22] have applied the DFT method using the GGA/PW91 functional with the double numerical plus d-functions basis set to investigate the adsorption behavior of three purine compounds, A, B and C on the Fe (0 0 1) surface. The theoretical results, including global molecular reactivity descriptors and active sites by Fukui functions analysis well support the order of the *IE*%. They also applied molecular dynamic simulation to predict the inhibitive performance of purines studied, the tested molecules adsorbed parallel onto Fe (0 0 1) surface, and the order of interaction energy support the experimental *IE*%. Using combined quantum chemical and molecular dynamic simulation studies, S. Kr. Saha et al. [23] also studied the adsorption characteristics of two aminobenzonitrile derivatives, (2-AB) and (3-AB) to understand the inhibition mechanism of steel corrosion in acidic medium (HCl).

**\*Corresponding author:** Quraishi MA, Department of Chemistry, Indian Institute of Technology, B.H.U. Varanasi, Uttar Pradesh, India-221005, Tel: 9307025126; E-mail: [maquraishi.apc@itbhu.ac.in](mailto:maquraishi.apc@itbhu.ac.in)

Received April 26, 2016; Accepted May 26, 2016; Published June 06, 2016

**Citation:** Lgaz H, Salghi R, Jodeh S, Ramli Y, Larouj M, et al (2016) Understanding the Adsorption of Quinoxaline Derivatives as Corrosion Inhibitors for Mild Steel in Acidic Medium: Experimental, Theoretical and Molecular Dynamic Simulation Studies. J Steel Struct Constr 2: 111. doi:10.4172/2472-0437.1000111

**Copyright:** © 2016 Lgaz H, et al. This is an open-access article distributed under the terms of the Creative Commons Attribution License, which permits unrestricted use, distribution, and reproduction in any medium, provided the original author and source are credited.

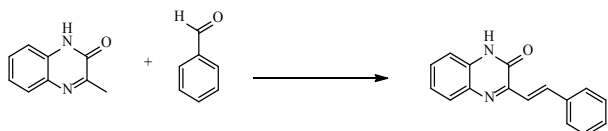
The quantum chemical parameters QCPs reveals that the electron donation and electron acceptance capability of 2-AB and 3-AB are in well accordance with experimental  $IE\%$ . While, the MD simulation reveals that the distance between active sites and Fe (1 0 0) atoms are lying within a range of 3.5 Å, indicating that a chemical bonds are formed during the interaction of the inhibitors on the Fe (1 1 0) surface. Recently, Z. Zhang et al. [24] applied the radial distribution function (RDF) to study the mechanism of adsorption processes and the synergistic inhibition effect between indigo carmine and three cationic molecules on CS, in an acidic solution. The researchers reported that the bonding length of all heteroatoms-Fe and carbons-Fe are less than 3.5 Å, suggesting that the adsorption of indigo carmine and their cationic molecules occur mainly by these atoms. In addition, Si-Wei Xie et al. [25] also introduced the RDF accompanying with DFT and experimental studies to investigate the inhibitive performance of 3,5-dibromo salicylaldehyde Schiff 's base. The results obtained revealed that C, N, O and S atoms of three studied inhibitors are the most reactive sites responsible of efficiency of the tested compound. This work aims to evaluate the inhibitory properties and adsorption characteristics of three synthetic quinoxaline derivatives of the MS in 1.0 M HCl, using the weight loss (WL), electrochemical techniques (EIS and PDP) and surface examination by SEM. Quantum chemical parameters (QCPs) by DFT method and Monte Carlo simulation accompanying with radial distribution function (RDF) of the (E)-3-styrylquinoxalin-2(1H)-one (STQ), (E)-1-benzyl-3-(4-methoxystyryl) quinoxalin-2(1H)-one (BMQ) and (E)-3-(2-(furan-2-yl) vinyl) quinoxalin-2(1H)-one (FVQ) were calculated and discussed.

## Data and Method

### Inhibitors preparation

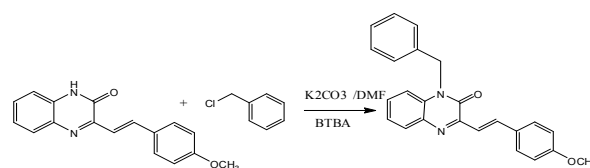
The tested inhibitors, namely (E)-3-styrylquinoxalin-2(1H)-one (STQ), (E)-1-benzyl-3-(4-methoxystyryl)quinoxalin-2(1H)-one (BMQ) and (E)-3-(2-(furan-2-yl)vinyl)quinoxalin-2(1H)-one (FVQ) were synthesized according to this experimental procedure:

The bibliography reports various methods to prepare styrylquinoxalines [26,27]. For our part, we suggested a different synthetic route which comprised reacting fusion 3-méthylquinoxaline-2-one with aromatic aldehydes. This method was carried out in the absence of solvent. We had a possibility to isolate the desired compound in a yield of around 80% (Scheme 1). Indeed, 6.25 mmol of 3-méthylquinoxaline-2-one was fused with 12.5 mmol of the benzaldehyde for 2 hours, at the boiling temperature of the latter. At the end of the reaction, the solid compound is allowed to cool and then heated at 100°C for 10 minutes in 50 ml of ethanol. The product is filtered hot then washed with ethanol [5,28] (Scheme 1).



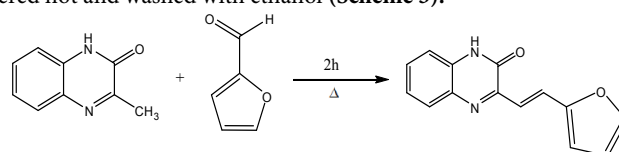
Scheme 1: Synthesis of (E)-3-styrylquinoxalin-2(1H)-one (STQ).

To a solution of (E)-3-(4-methoxystyryl)quinoxalin-2(1H)-one in 20 ml of dimethyl formaldehyde was added (chloromethyl) benzene (0.85 ml),  $K_2CO_3$  (1 g) and catalytic amount of tetrabutylammoniumbromide. The mixture was stirred at room temperature for 24 h. Then the solvent was remove under reduce pressure, the residue was crystallized in ethanol to afford the (E)-1-allyl-3-(4-methoxystyryl) quinoxalin-2(1H)-one [29]. (Scheme 2).



Scheme 2: Synthesis of (E)-1-benzyl-3-(4-methoxystyryl) quinoxalin-2(1H)-one (BMQ).

6.25 mmol of 3-méthylquinoxalin-2(1H)-one was merged with 12.5 mmol of the furan-2-carbaldehyde for 2 h, at the boiling temperature of the latter. At the end of the reaction, the solid was allowed to cool and then heated to 100°C for 10 min in 50 ml of ethanol. The product was filtered hot and washed with ethanol (Scheme 3).



Scheme 3: Synthesis of (E)-3-(2-(furan-2-yl) vinyl) quinoxalin-2(1H)-one (FVQ).

**Electrolytic solution and concentration range:** Acid solutions (1.0 M HCl) were prepared by diluting a reagent of analytical grade HCl 37% (from Sigma-Aldrich) with double-distilled water. The concentration range of the quinoxaline derivatives used was 2 to 8 mM.

**Weight loss tests, electrochemical measurements and surface observation:** In this study, the effects of quinoxaline derivatives (BMQ, FVQ and STQ) on the metal corrosion were performed by the electrochemical measurements (EIS and polarization curves), and weight loss (WL) tests (temperature range of 303 to 333 K). The detail of experiments referenced from the published article of Rachid Salghi et al. [4,30,31].

**Molecular modeling and dynamic simulations:** All quantum chemical calculations of quinoxaline derivatives were performed at the DFT/B3LYP level of theory using 6-31G (d, p) basis set with Gassian03 program [32-35]. The adsorption configuration of BMQ, FVQ and STQ on iron surface were dynamically simulated by using the Adsorption Locator module of the Materials Studio 6.0 software from Accelrys Inc [36]. The Fe crystal was chosen to represent the MS surface. First the crystal was cleaved along the (1 1 0) plane, as it is the most stable surface as reported in the literature [37]. Then, the Fe (1 1 0) plane was subsequently enlarged into an appropriate supercell to provide a large surface for the interaction of the inhibitor. The interaction between BMQ, FVQ, STQ and Fe surface was assumed in a simulation box (29.78 × 29.78 × 60.13 Å) with periodic boundary conditions. After that, thickness of the vacuum slab was 50 Å. COMPASS force field was chosen to optimize the structures of all components of the system of interest. More detail of MC simulation is referenced from the published articles [37,38].

## Results and Discussion

### Weight loss measurement

**Effect of concentration and temperature:** The inhibitive efficiency calculated by the Eq. (1) of BMQ, FVQ and STQ in the corrosive medium of the MS was carried out after immersion for 6 h at 303 to 333 K, in all studied concentrations by weight loss measurements. The results are presented in Table 1 and Figure 1 (Similar plots obtained for 313-333 K, but not presented in this article).

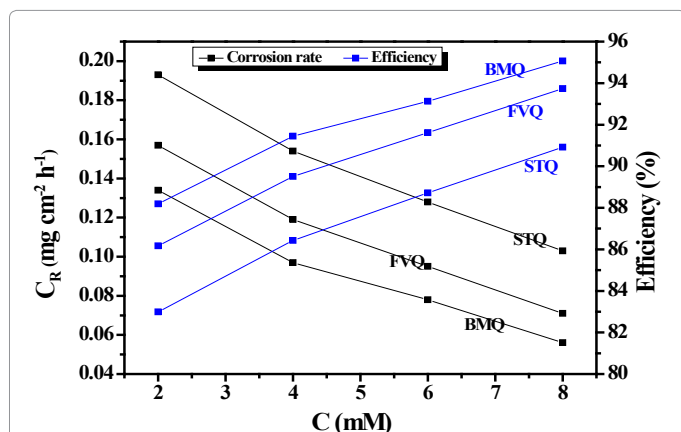


Figure 1: Relationship between the inhibition efficiency, corrosion rate and inhibitors concentration for MS after 6 h immersion in 1.0 M HCl at 303 K.

Temp. (K)	Concentration (mM)	BMQ		FVQ		STQ	
		C <sub>R</sub> (mg cm <sup>-2</sup> h <sup>-1</sup> )	η <sub>w</sub> (%)	C <sub>R</sub> (mg cm <sup>-2</sup> h <sup>-1</sup> )	η <sub>w</sub> (%)	C <sub>R</sub> (mg cm <sup>-2</sup> h <sup>-1</sup> )	η <sub>w</sub> (%)
303	Blank	1.135	-	-	-	-	-
	8	0.056	<b>95.07</b>	0.071	<b>93.74</b>	0.103	<b>90.92</b>
	6	0.078	93.13	0.095	91.62	0.128	88.72
	4	0.097	91.45	0.119	89.51	0.154	86.43
	2	0.134	88.19	0.147	87.04	0.174	84.66
313	Blank	2.466	-	-	-	-	-
	8	0.157	<b>93.63</b>	0.201	<b>91.85</b>	0.311	<b>87.39</b>
	6	0.197	92.01	0.262	89.37	0.361	85.36
	4	0.293	88.12	0.343	86.09	0.426	82.72
	2	0.341	86.17	0.385	84.38	0.501	79.68
323	Blank	5.032	-	-	-	-	-
	8	0.446	<b>91.14</b>	0.521	<b>89.65</b>	0.794	<b>84.22</b>
	6	0.546	89.15	0.647	87.14	0.898	82.15
	4	0.765	84.79	0.801	84.08	1.058	78.97
	2	0.897	82.17	1.008	79.96	1.178	76.59
333	Blank	10.029	-	-	-	-	-
	8	1.192	<b>88.11</b>	1.527	<b>84.77</b>	1.812	<b>81.93</b>
	6	1.388	86.16	1.758	82.47	2.081	79.25
	4	1.793	82.12	2.196	78.1	2.345	76.62
	2	2.329	76.77	2.532	74.75	2.901	71.07

Table 1: C<sub>R</sub> and η<sub>w</sub> % obtained from weight loss measurements of MS in 1 M HCl containing various concentrations of BMQ, FVQ and STQ at different temperatures.

$$\eta_w (\%) = \frac{C_R - C_{R(inh)}}{C_R} \times 100 \quad (1)$$

C<sub>R</sub> and C<sub>R(inh)</sub> are the corrosion rates in the absence and presence of BMQ, FVQ and STQ, respectively.

Prominent decrease of the C<sub>R</sub> observed because of the addition of various concentrations of quinoxaline derivatives, while the IE% increases with increasing the concentration of tested inhibitors at the range of studied temperature. Over temperature increase the IE% of our molecules is reduced due to partial desorption of studied compounds. The IE% values of BMQ decreased slowly (95.07% to 88.19% in 8 mM) compared with those of FVQ and STQ (η<sub>w</sub> % reduced to 86.17% for FVQ and 82.99% for STQ) following the order: BMQ > FVQ > STQ. This can be attributed to the difference in molecular

size of quinoxaline compounds. The high protection of our molecules is due to their adsorption on steel surface, which decreases the fatal effect of aggressive medium.

**Activation parameters:** The inhibitive mechanism can be understood based on the thermodynamic and activation parameters. From Table 1, it can be observed that C<sub>R</sub> depends on temperature for all inhibitor concentrations. The C<sub>R</sub> is related to the temperature by the following Eqs. (2,3) [39]:

$$C_R = k \exp\left(\frac{-E_a}{RT}\right) \quad (2)$$

$$C_R = \frac{RT}{Nh} \exp\left(\frac{\Delta S_a}{R}\right) \exp\left(-\frac{\Delta H_a}{RT}\right) \quad (3)$$

where, E<sub>a</sub> is the activation energy, ΔS<sub>a</sub> is the change in entropy of activation, ΔH<sub>a</sub> is the change in enthalpy of activation, k is the Arrhenius pre-exponential factor, h is Planck's constant, N is Avogadro's number, T is the absolute temperature and R is the universal gas constant.

Using Eq. (2) a plot of ln C<sub>R</sub> versus 1/T were drawn to get a straight line (Figure 2), from the values of slope and intercept, the values of E<sub>a</sub> were calculated for three inhibitors at various concentrations. Using Eq. (3), another linear plot of ln C<sub>R</sub>/T versus 1/T was drawn (Figure 3) with slope (-ΔH<sub>a</sub>/R) and intercept [ln(R/Nh) + ΔS<sub>a</sub>/R], which were used for the calculation of ΔH<sub>a</sub> and ΔS<sub>a</sub>. All the values are listed in Table 2. We can be find from Table 2 that the Ea (Inh) > Ea (Blank), which can be explained by the physical adsorption of quinoxaline molecules [40]. For three inhibitors, the value of the activation energy to take up higher maximum for the higher concentrations; and generally follows the order of Ea (BMQ) > Ea (FVQ) > Ea (STQ), this order is in good agreement with the order of inhibition efficiencies, that decreased with the increase of the temperature. In the same case, Saranya et al. [17] studied the inhibition effect of Acenaphtho[1,2-b] quinoxaline on the MS dissolution in acidic environment, the effect of temperature study reveals that the IE% decrease with the increase of the temperature and the E<sub>a</sub> value decrease remarkably than the value obtained in blank solution, which in good correlation with our investigation (Figure 4).

The positive sign of the enthalpy (Table 2) reflects the endothermic nature of the MS dissolution process. While the higher values of ΔS<sub>a</sub> in presence of investigated compounds compared to those calculated from the uninhibited solution might be the result of the adsorption of quinoxaline derivatives from the aggressive solution, which could be regarded as a quasi-substitution process between inhibitor molecules in the aqueous phase and water molecules on the MS surface [41,42].

### Adsorption isotherm and thermodynamic parameters

On the basis of evaluation of the interaction between the inhibitors and steel surface, it is important to consider the adsorption isotherms to analyze the mechanism and nature of the adsorption processes of chemicals species on the MS surface [43]. For additional information about the compounds tested, several types of adsorption isotherms carried out such as Frumkin (Eq. 4), Temkin (Eq. 5), Freundlich (Eq. 6) and Langmuir (Eq. 7) among which the Langmuir isotherm showed the best fit with regression coefficient (R<sup>2</sup>) values close to unity for all tested compounds. Considering a sufficient time for adsorption equilibrium, the fractional surface coverage (θ) can be easily calculated by η<sub>w</sub> (%) / 100 from weight loss tests [44]:

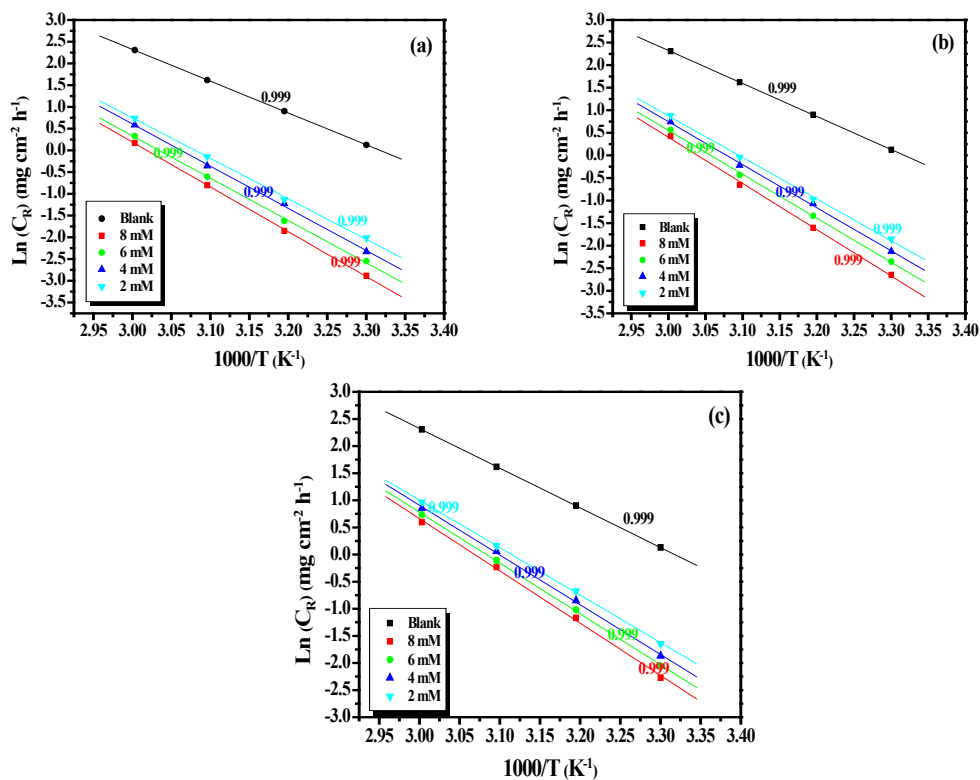


Figure 2: Arrhenius plots for the MS in 1.0 M HCl in the absence and presence of different concentrations of (a) BMQ (b) FVQ and (c) STQ at different temperatures.

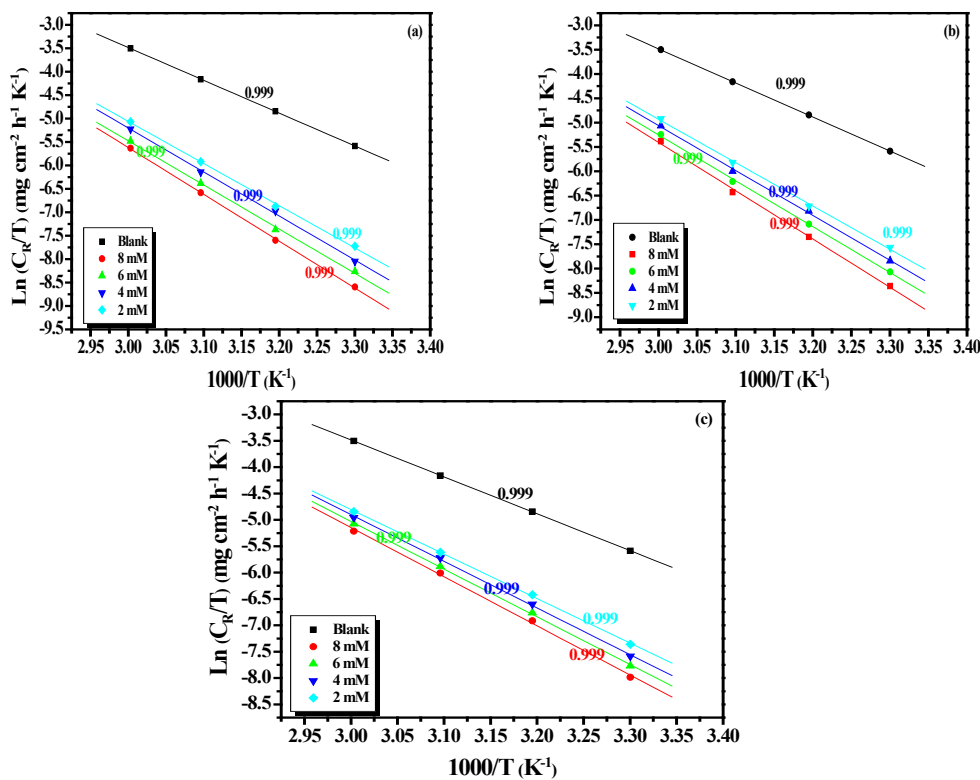


Figure 3: Transition state plots for the inhibition of corrosion of the MS in 1.0 M HCl in the absence and presence of different concentrations of (a) BMQ (b) FVQ and (c) STQ at different temperatures.

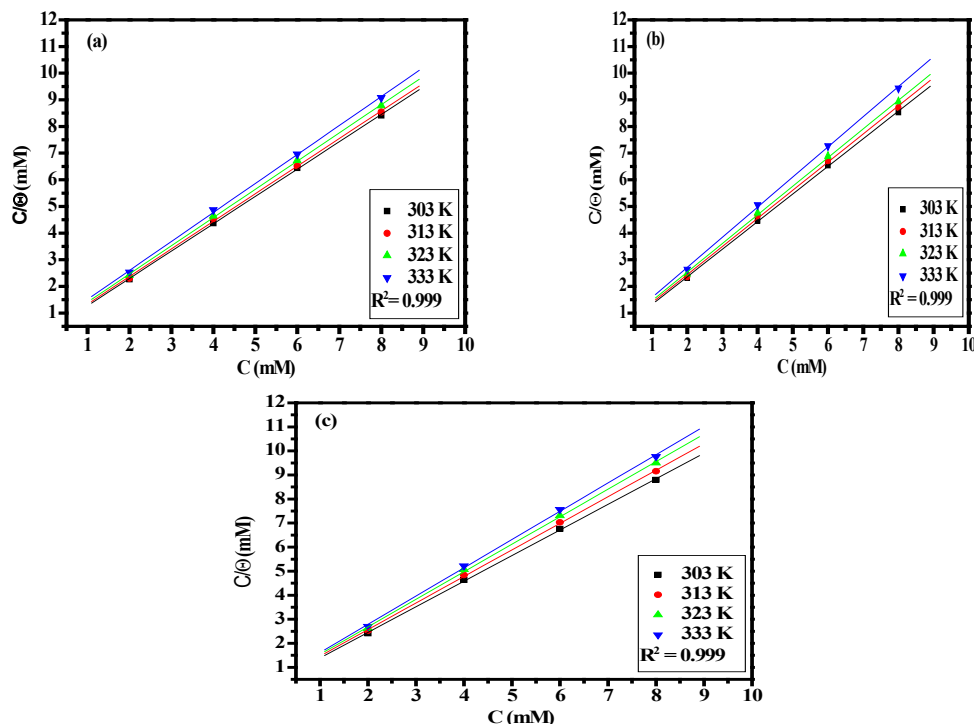


Figure 4: Langmuir adsorption isotherm on the MS in 1.0 M HCl at different temperatures of (a) BMQ (b) FVQ and (c) STQ.

Inhibitors	Concentration (mM)	Ea (kJ mol <sup>-1</sup> )	ΔHa (kJ mol <sup>-1</sup> )	ΔSa (kJ mol <sup>-1</sup> K <sup>-1</sup> )	Ea-ΔHa
Blank	-	60.79	58.15	-51.84	2.64
BMQ	8	85.65	83.01	5.07	2.64
	6	80.92	78.28	-8.04	2.64
	4	80.68	78.04	-6.46	2.64
	2	77.44	74.80	-15.01	2.64
FVQ	8	85.10	82.46	5.05	2.64
	6	80.94	78.30	-6.10	2.64
	4	79.30	76.66	-9.43	2.64
	2	76.66	74.02	-16.28	2.64
STQ	8	80.09	77.45	-7.78	2.64
	6	77.84	75.20	-13.54	2.64
	4	76.20	73.56	-17.41	2.64
	2	72.72	70.08	-27.05	2.64

Table 2: Activation parameters for MS corrosion in 1.0 M HCl in the absence and presence of different concentrations of BMQ, FVQ and STQ at different temperatures.

$$\theta = \frac{1}{f} \ln \left( K_{ads} \frac{C(1-\theta)}{C} \right) \quad (4)$$

$$\theta = \frac{1}{f} \ln (K_{ads} C) \quad (5)$$

$$\theta = K_{ads} C \quad (6)$$

$$\frac{C}{\theta} = \frac{1}{K_{ads}} + C \quad (7)$$

Where: C is the concentration of inhibitors in the electrolyte,  $K_{ads}$  is the equilibrium constant for the adsorption-desorption process,  $\theta$  is

the surface coverage and f is the molecular interaction constant. The values of  $K_{ads}$  can be calculated from the intercepts of the straight lines  $C_{inh}/\theta$ -axis. The  $K_{ads}$  related to the standard free energy of adsorption  $\Delta G_{ads}^{\circ}$  by following Eq. (8):

$$\Delta G_{ads}^{\circ} = -RT \ln (C_{solvent} \times K_{ads}) \quad (8)$$

Where:  $C_{solvent}$  is the molar concentration of solvent (For  $H_2O$  is 55.5 mol L<sup>-1</sup>), T is the absolute temperature. The  $K_{ads}$  and  $\Delta G_{ads}^{\circ}$  values calculated and collected in Table 3. The values of  $K_{ads}$  could take as an indication of the adsorption ability of BMQ, FVQ and STQ on the steel surface. On the other hand, the  $K_{ads}$  values follow the order:  $K_{ads} (BMQ) > K_{ads} (FVQ) > K_{ads} (STQ)$ . This further confirms that  $n_w$  (%) decreases with the increase in temperature and the better inhibitive performance of BMQ than the others compounds. The negative values of  $\Delta G_{ads}^{\circ}$  imply that the adsorption was spontaneous and the stability of the adsorbed film on the MS surface [45]. All the  $\Delta G_{ads}^{\circ}$  values are around -13 kJ/mol. normally, the physical adsorption is correlated with the absolute values of  $\Delta G^{\circ}$  around 20 kJ/mol or lower, and a value of  $\Delta G_{ads}^{\circ}$  up to 40 kJ/mol or more negative is an indication of the chemical adsorption [46,47]. The  $\Delta G_{ads}^{\circ}$  values in Table 3 indicate clearly the physical adsorption of tested compounds on the MS surface. In the literature, we can find in the investigation of Obot et al. [17] that the 2,3-Diphenylbenzoquinoxaline interact with the MS in the same way in sulphuric acid, the authors reported that the  $\Delta G_{ads}^{\circ}$  is -11.4 kJ mol<sup>-1</sup>, which explained by the electrostatic interaction with tested quinoxaline derivative and the MS surface. The  $\Delta H_{ads}$  and  $\Delta S_{ads}$  calculated by the following Eq. (9):

$$\ln K_{ads} = \ln \frac{1}{55.5} - \frac{\Delta H_{ads}^{\circ}}{RT} + \frac{\Delta S_{ads}^{\circ}}{R} \quad (9)$$

The values of  $\Delta H_{ads}$  and  $\Delta S_{ads}$  are collected in Table 3, more information of the corrosion process and nature of adsorption can be obtained on the basis of the values of  $\Delta H_{ads}^{\circ}$  of investigated compounds. The  $\Delta H_{ads}^{\circ}$  values of quinoxaline derivatives are negative, indicating the exothermic process of adsorption of studied inhibitors. The endothermic adsorption process  $\Delta H_{ads}^{\circ} > 0$  is correlated to chemical adsorption, while the exothermic adsorption process  $\Delta H_{ads}^{\circ} < 0$  is attributed to physical, chemical or mixture adsorption [48]. In an exothermic process, the physisorption process is correlated with the values of  $\Delta H_{ads}^{\circ}$  lower than  $40 \text{ kJ mol}^{-1}$ . Whereas, chemical adsorption is for  $\Delta H_{ads}^{\circ}$  values around  $100 \text{ kJ mol}^{-1}$ . In this investigation,  $\Delta H_{ads}^{\circ}$  values of all quinoxalines derivatives are less than  $40 \text{ kJ mol}^{-1}$ , suggesting that the physical adsorption may occur during the interaction between the tested compounds and the MS surface. The negative values of  $\Delta S_{ads}$  indicates that before the adsorption of inhibitor's molecules on the MS surface, inhibitor molecules might freely move in the bulk solution, but with the progress in the adsorption of **BMQ**, **FVQ** and **STQ**, inhibitors molecules were orderly adsorbed on the MS surface, as a result a decrease in entropy is observed [49]. Based on the thermodynamic principles, it can be noted that since the adsorption is an exothermic process, it must be accompanied by a decrease of entropy [50].

### Potentiodynamic polarization study

The polarization experiments were undertaken to distinguish the behavior of the corrosion of the MS with and without studied concentrations of **BMQ**, **FVQ** and **STQ** at 303 K. The Tafel plots and the derived parameters are presented in Figures 5a-5c and Table 4, respectively. The  $IE\%$  is calculated using the following Eq. (10) [51,52]:

$$\eta_{PDP} (\%) = \frac{I_{corr} - I_{corr(i)}}{I_{corr}} \times 100 \quad (10)$$

Where  $I_{corr}$  and  $I_{corr(i)}$  are the corrosion current densities for the MS in 1.0 M HCl and in 1.0 M HCl with various concentrations of the tested compounds, respectively.

It can be observed from Figures 5a-5c, that the addition of quinoxaline derivatives caused a decrease in the anodic and cathodic current densities with slight shifting of the corrosion potential ( $E_{corr}$ ), indicating that the quinoxaline derivatives investigated are mixed type inhibitors [53,54]. The small change of the constant cathodic Tafel slope,  $\beta_c$ , suggests that the mechanism of proton discharge reaction does not modify by addition of quinoxaline derivatives [55,56]. From Table 4, it can be found that the increase of the concentration of our molecules result in a considerable decrease of the  $I_{corr}$  values. In the same trend, a remarkable increase of the  $IE\%$  is observed when increasing the inhibitors concentration reaching a maximum value at 8 mM in the three quinoxaline derivatives studied. It is also evident that **BMQ** presents the better performance than other inhibitors, which can be correlated to the difference of the structure of the three inhibitors molecules (Figure 6).

### AC impedance study

Nyquist plots of the MS in acidic solutions with and without various concentrations of **STQ**, **FVQ** and **BMQ** at 303 K after 30min of immersion are given in Figures 7a-7c. Which a single capacitive loop is clearly observed over the frequency range studied [57,58]. Also appearing are depressed Nyquist plots into the real axis and imperfect semicircles, what can explained by the non-homogeneity and roughness of the MS surface [59]. As previously reported for steel/acid interface, the  $EIS$  data obtained was fitted using the Rs(CPE/Rct) equivalent circuit (Figures 8 and 9) [60], where Rs is the solution

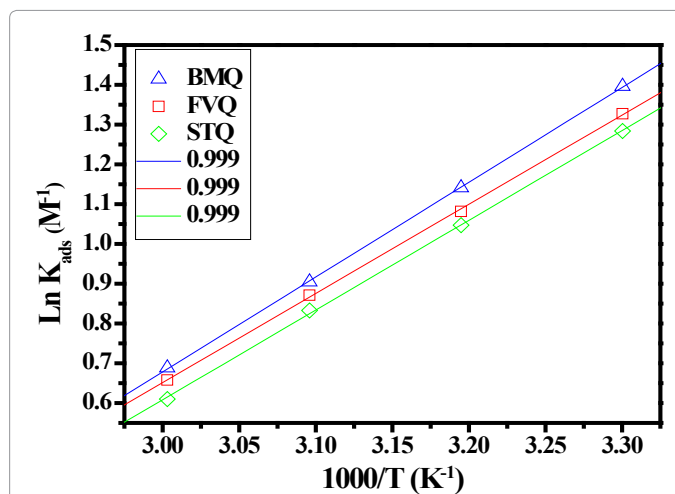


Figure 5: Plots of  $\text{Ln } K_{ads}$  vs  $1/T$  for the inhibition of corrosion of MS in 1.0 M HCl with inhibitors.

Inhibitors	Temperature (K)	$K_{ads}$ ( $M^{-1}$ )	$\Delta G_{ads}$ ( $\text{kJ mol}^{-1}$ )	$\Delta H_{ads}$ ( $\text{kJ mol}^{-1}$ )	$\Delta S_{ads}$ ( $\text{J mol}^{-1}\text{K}^{-1}$ )
<b>BMQ</b>	303	4.04	-13.62	-19.81	-20.41
	313	3.13	-13.41		
	323	2.47	-13.21		
	333	1.99	-13.01		
<b>FVQ</b>	303	3.77	-13.45	-18.61	-17.04
	313	2.95	-13.26		
	323	2.39	-13.11		
	333	1.93	-12.93		
<b>STQ</b>	303	3.61	-13.34	-18.59	-17.81
	313	2.85	-13.17		
	323	2.30	-13.01		
	333	1.84	-12.80		

Table 3: Adsorption parameters of **BMQ**, **FVQ** and **STQ** for mild steel corrosion in 1.0 M HCl at different temperatures.

Inhibitor	Concentration (mM)	$-E_{corr}$ (mV/SCE)	$-\beta_c$ (mV/dec $^{-1}$ )	$I_{corr}$ ( $\mu\text{A cm}^{-2}$ )	$\eta_{Tafel}$ (%)	$\theta$
Blank	1.0	496	150.19	564	-	-
<b>BMQ</b>	8	499	146.79	20.98	<b>96.28</b>	0.9628
	6	525	145.61	38.12	93.24	0.9324
	4	532	144.60	56.21	90.03	0.9003
	2	539	147.00	68.04	87.94	0.8794
<b>FVQ</b>	8	513	145.34	30.08	<b>94.67</b>	0.9467
	6	530	146.66	50.67	91.01	0.9101
	4	544	141.37	71.59	87.31	0.8731
	2	555	147.73	85.18	84.90	0.8490
<b>STQ</b>	8	526	135.19	47.03	<b>91.66</b>	0.9166
	6	539	134.24	59.32	89.48	0.8948
	4	552	137.27	88.00	84.40	0.8440
	2	547	139.13	106.04	81.20	0.8120

Table 4: Corrosion parameters for corrosion of MS with selected concentrations of the inhibitors in 1.0 M HCl by potentiodynamic polarization method at 303K.

resistance,  $R_{ct}$  denotes that the charge-transfer resistance and CPE is "constant phase element". The introduction of CPE was necessitated to compensate deviations from ideal capacitor due to distributed surface heterogeneity. The impedance of this element is frequency-dependent and can be calculated using the Eq. (11) [61,62]:

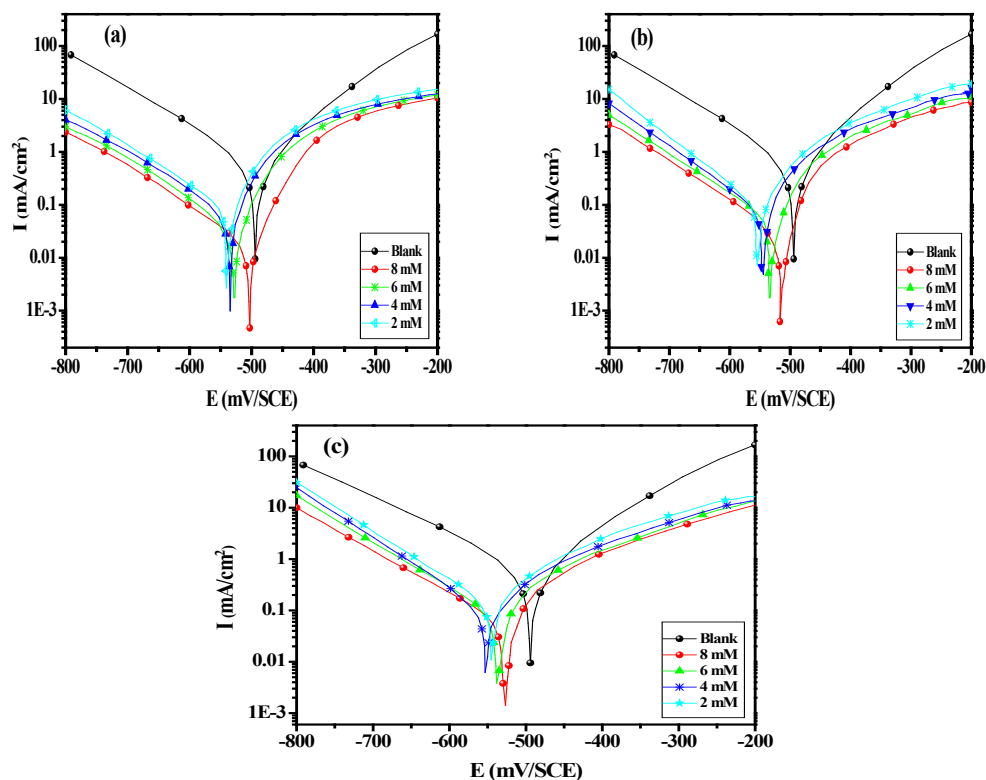


Figure 6: Polarisation curves of MS in 1.0 M HCl for various concentrations of the inhibitors: (a) BMQ, (b) FVQ and (c) STQ at 303K.

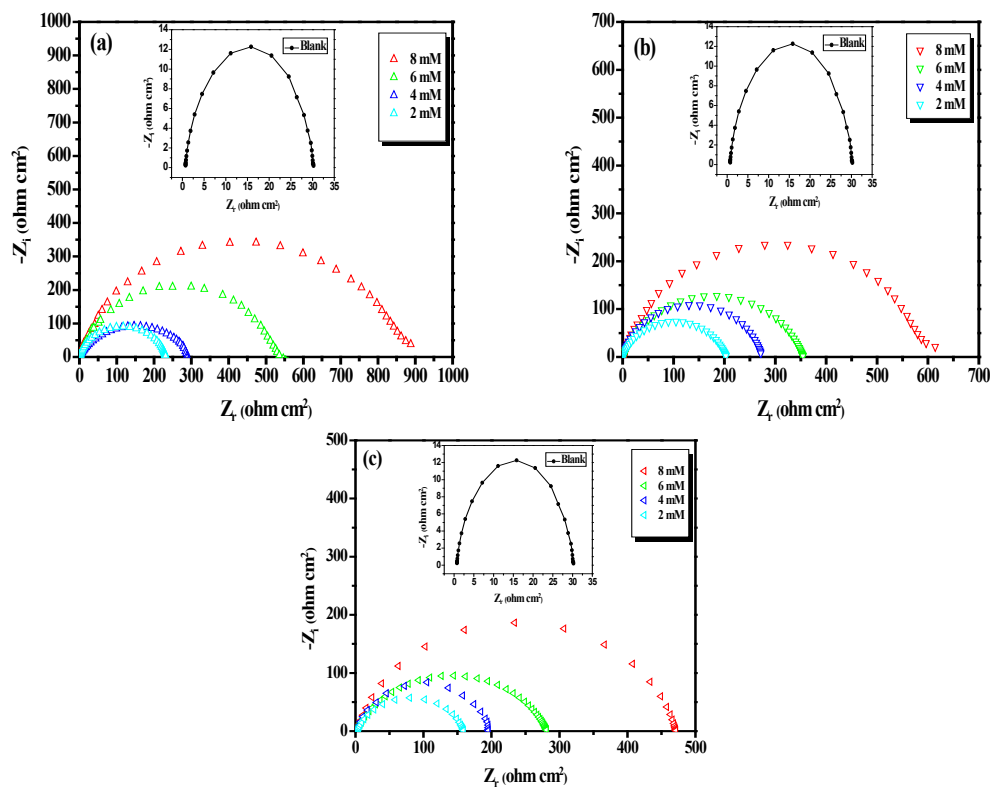


Figure 7: Nyquist curves for MS in 1.0 M HCl for selected concentrations of the inhibitors: (a) BMQ, (b) FVQ, and (c) STQ at 303K.

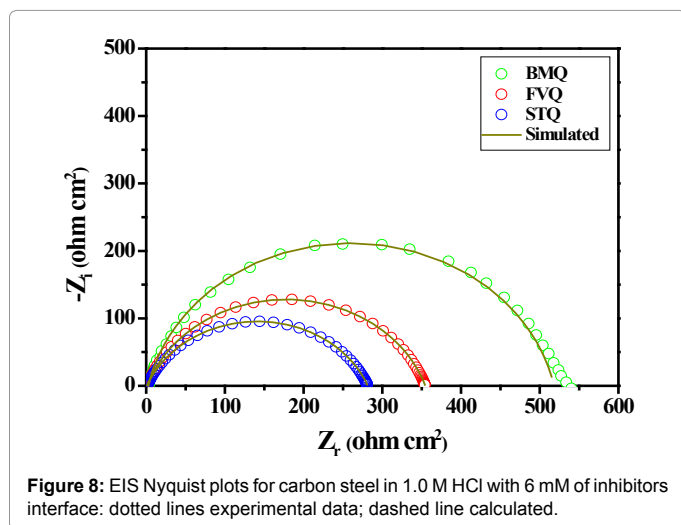


Figure 8: EIS Nyquist plots for carbon steel in 1.0 M HCl with 6 mM of inhibitors interface: dotted lines experimental data; dashed line calculated.

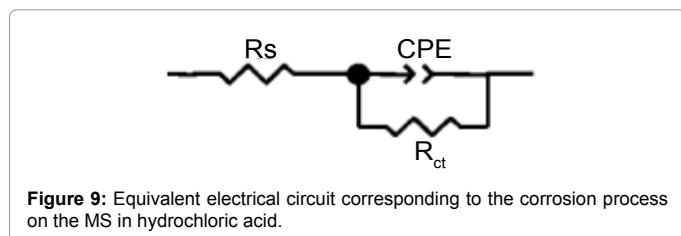


Figure 9: Equivalent electrical circuit corresponding to the corrosion process on the MS in hydrochloric acid.

$$Z_{CPE} = \frac{1}{Q(j\omega)^n} \quad (11)$$

Where  $Q$  is the CPE constant (in  $\Omega^{-1} S^n cm^{-2}$ ),  $\omega$  is the angular frequency (in  $rad s^{-1}$ ),  $j^2 = -1$  is the imaginary number and  $n$  is a CPE exponent which can be used as a gauge for the heterogeneity or roughness of the surface [63]. The electrochemical parameters derived from the fitting of impedance spectra are collected in Table 5. The  $IE\%$  was calculated by the Eq. (12):

$$\eta_{EIS} (\%) = \left( \frac{R_{ct} - R_{ct}^0}{R_{ct}} \right) \times 100 \quad (12)$$

Where:  $R_{ct}^0$  and  $R_{ct}$  are the charge transfer resistances without and with various concentrations of inhibitors respectively. According to the values of  $R_{ct}$  displayed in Table 5, the  $R_{ct}$  value increase considerably with rising in inhibitors concentration (from 231.1 to 847.1  $\Omega$  for **BMQ**) resulting in a slower corrosion of steel due to the adsorption of quinoxaline derivatives on metal surface [64,65]. Regarding, the double layer capacitances,  $C_{dl}$  is associated with a CPE by the following Eq.(13) [66]:

$$C_{dl} = \left( Q \cdot R_{ct}^{1-n} \right)^{1/n} \quad (13)$$

The  $C_{dl}$  values were decreased, so that the  $C_{dl}$  values reached 15.09  $\mu F cm^{-2}$  for **BMQ**, 18.48  $\mu F cm^{-2}$  for **FVQ** and 21.07  $\mu F cm^{-2}$  for **STQ** considering 85.89  $\mu F cm^{-2}$  for the uninhibited solution. On the other side, the values of the proportional factor  $Q$  of CPE increase when decreasing the concentration of the quinoxaline derivatives. These results are probably correlated with the adsorption of the three inhibitors on steel surface [66,67]. Accordingly, the values of  $n$  lies between 0.89 and 0.92 for inhibited solutions, the addition of quinoxaline derivatives increased  $n$  values, indicating the increase in in-homogeneity of the MS surface, due to the adsorption of the our inhibitors [68,69].

The inhibition efficiency values in the absence and presence of **BMQ**, **FVQ** and **STQ** yielded 96.53%, 94.98% and 93.73% in the highest concentrations, respectively with the following order: **BMQ** > **FVQ** > **STQ**. This order can be explained by the presence of a phenyl and (-OCH<sub>3</sub>) in **BMQ**, which raised their reactivity.

### SEM analysis

SEM photomicrographs of the surface of MS were immersed for 6 h in a corrosive medium with and without 8 mM of **STQ**, **BMQ** and **FVQ**. Results are displayed in Figures 10a-10e. In acidic environment, obvious dissolution can be observed without the presence of any inhibitors. In presence of **BMQ**, **FVQ** and **STQ**, it can be seen (Figures 10a-10c) that the surface of the MS was improved, smooth, and that less pits and less damage was observed, This demonstrates the formation of insoluble film, resulting from the adsorption of **BMQ**, **FVQ** and **STQ** on the MS surface. These observations support the high inhibition performance of the quinoxaline derivatives.

### Quantum chemical calculations

**Global molecular reactivity:** We attempted to interpret the main factors responsible for the reactivity of the investigated quinoxaline derivatives and to analyse the capability of our molecules to donate and accept electrons to/and from the MS surface. The optimized structures of the quinoxaline derivatives molecules were calculated and presented in Figure 11. The QCPs such as  $E_{HOMO}$ ,  $E_{LUMO}$ ,  $\Delta E = (E_{LUMO} - E_{HOMO})$ , total energy (TE), softness ( $\sigma$ ), the fraction of electrons transferred ( $\Delta N$ ) and dipole moment ( $\mu$ ) were collected in Table 6. The  $IE\%$  of **BMQ**, **FVQ** and **STQ** according to our experimental studies is:

$$BMQ > FVQ > STQ$$

In Figure 11, The HOMO and LUMO orbitals are distributed over the entire quinoxaline molecules, resulting in the highest interaction of quinoxaline derivatives studied on the MS surface. This observation also suggests that the heteroatoms and the cycle rings containing  $\pi$ -bonds are the probable reactive sites for adsorption of inhibitors on the metal surface. Normally,  $E_{HOMO}$  is often indicated the ability of a molecule to donate electrons; this ability becomes more considerable with a high value of  $E_{HOMO}$ . While, the lowering of  $E_{LUMO}$  is often associated with the capability of an inhibitor to accept electrons [70,71]. The  $\Delta E = (E_{LUMO} - E_{HOMO})$  was reported as a main chemical reactivity factor of an inhibitor from theoretical point of view [71]. According to these literature findings and the results from Table 6, it can be observed that our compounds have higher interactions with the steel surface. The reactivity of **BMQ**, **FVQ** and

Inhibitor	Conc (M)	$R_{ct}$ ( $\Omega cm^2$ )	$n$	$Q \times 10^4$ ( $s^n \Omega^{-1} cm^{-2}$ )	$C_{dl}$ ( $\mu F cm^2$ )	$\eta_z$ (%)	$\theta$
Blank	1.0	29.35	0.88	1.7610	85.89	-	-
BMQ	8	847.1	0.92	0.2139	15.09	<b>96.53</b>	0.9653
	6	515.2	0.89	0.2870	17.05	94.30	0.9430
	4	301.3	0.91	0.3354	21.29	90.25	0.9025
	2	231.1	0.93	0.4112	28.96	87.29	0.8729
FVQ	8	585.2	0.92	0.2655	18.48	<b>94.98</b>	0.9498
	6	353.4	0.92	0.2889	19.39	91.69	0.9169
	4	273.3	0.93	0.3702	26.20	89.26	0.8926
	2	203.3	0.91	0.4812	30.45	85.56	0.8556
STQ	8	468.8	0.93	0.2911	21.07	<b>93.73</b>	0.9373
	6	280.7	0.91	0.3546	22.48	89.54	0.8954
	4	192.3	0.92	0.4132	27.14	84.73	0.8473
	2	156.2	0.91	0.5170	32.10	81.20	0.8120

Table 5: AC-impedance parameters for corrosion of MS for selected concentrations of the inhibitors in 1.0 M HCl at 303K.

Molecule	$E_{HOMO}$ (eV)	$E_{LUMO}$ (eV)	$\Delta E$ (eV)	$\mu$ (eV)	TE(eV)	$\eta$ (eV)	$\sigma$ (eV <sup>-1</sup> )	$\chi$ (eV)	$\Delta N$	IE (%)
BMQ	-3.7557	-1.0245	2.7312	2.3105	-1111.9	1.3656	0.7323	2.3901	0.6114	96.53
FVQ	-5.4151	-2.2308	3.1843	2.1136	-799.5	1.5922	0.6281	3.8229	0.0744	94.98
STQ	-5.6441	-2.2650	3.3791	2.2391	-801.6	1.6895	0.5918	3.9546	0.0312	93.73

Table 6: Calculated quantum chemical parameters of the inhibitors molecules.

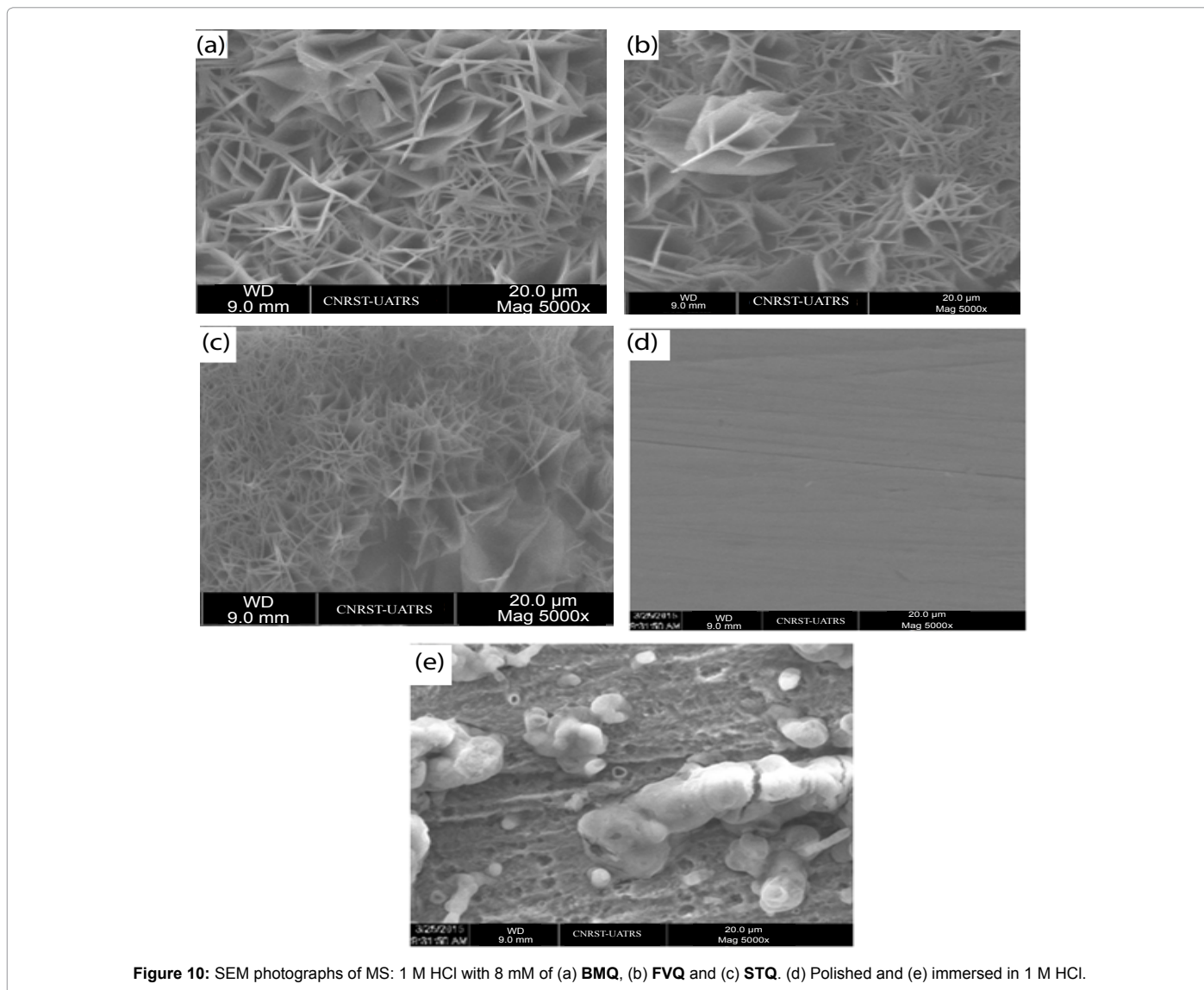


Figure 10: SEM photographs of MS: 1 M HCl with 8 mM of (a) BMQ, (b) FVQ and (c) STQ. (d) Polished and (e) immersed in 1 M HCl.

STQ can be classified by the following order:

$$BMQ > FVQ > STQ$$

Recently, Olasunkanmi et al. [14] employed four quinoxaline derivatives, noted Me-4-PQPB, Mt-4-PQPB, Mt-3-PQPB and Oxo-1,3-PQPB to study the corrosion inhibition of MS in hydrochloric acid medium, the authors reported that the IE% values at optimum concentration are 80.42%, 72.01%, 69.66% and 68.41% respectively. While, in the theoretical calculations the  $\Delta E$  values are found to be 3.55, 3.93, 3.93 and 3.67, these results further support the inhibitive performance of our compounds.

The absolute electronegativity ( $\chi$ ) and global hardness ( $\eta$ ) of the inhibitors molecule are approximated as follows [72,73]:

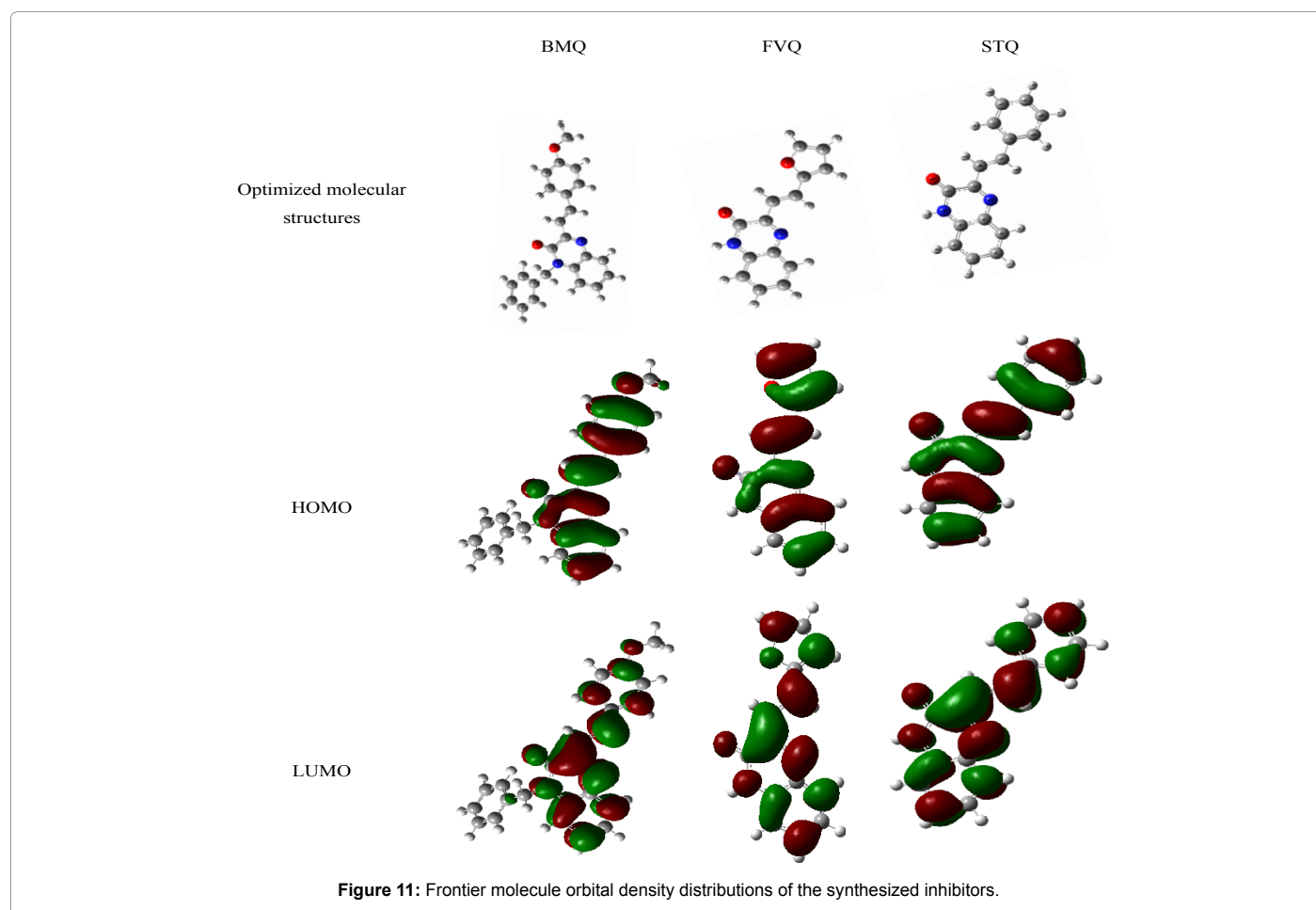
$$\chi = \frac{I + A}{2} \quad (14)$$

$$\eta = \frac{I - A}{2} \quad (15)$$

Where:  $I = -E_{HOMO}$  and  $A = -E_{LUMO}$

Thus the fraction of electrons transferred from the inhibitor to metallic surface,  $\Delta N$ , is given by [74]:

$$\Delta N = \frac{\chi_{Fe} - \chi_{inh}}{2(\eta_{Fe} + \eta_{inh})} \quad (16)$$

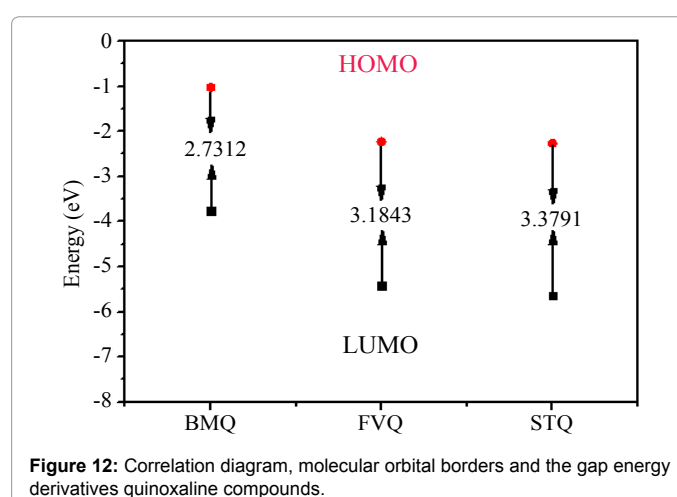


- The theoretical values of  $\chi_{\text{Fe}}$  ( $4.06 \text{ eV mol}^{-1}$ ) and of  $\eta_{\text{Fe}}$  ( $0 \text{ eV mol}^{-1}$ ) are used to calculate  $\Delta N$  [75,76]. The results from Table 6, show that the order of electron transfer is such that **BMQ** > **FVQ** > **STQ** which also confirms that **BMQ** has the highest tendency to donate electrons and therefore the highest tendency to bind onto the metal surface [76,77].

The hard-soft-acid-base (HSAB) theory introduced by Pearson [78] can be used in correlation with the *FMO* theory to understanding the tendencies of the inhibitors to bonding towards the MS atoms [79]. According to HSAB theory, hard acids prefer to co-ordinate to hard bases to give ionic complexes and soft acids prefer binding to soft bases to give covalent complexes. On the other hand, metal atoms are definite as soft acids. Hard molecules have a high value of  $\Delta E_{\text{HOMO-LUMO}}$ . In contrast, soft molecules have a small  $\Delta E_{\text{HOMO-LUMO}}$  [80]. Thus soft base compounds are the most capable to bind with metal atoms. So, the **BMQ** compound which has the lowest  $\Delta E_{\text{HOMO-LUMO}}$  and the highest softness has mostly been confirmed by calculating the softness,  $\sigma$ , to measures the reactivity of a molecule:  $\sigma = 1/\eta$ , (Table 6). It was observed that **BMQ** compounds have the highest  $\sigma$  value and the order at which softness increases, so that the reactivity will be:

$$\text{BMQ} > \text{FVQ} > \text{STQ}$$

Figure 12 shows the relationship between the *FMO* of quinoxaline compounds studied and their energy gap  $\Delta E_{\text{g}}$ . **BMQ**, **FVQ** and **STQ** have low energy gap, which facilitate their adsorption. The order of the reactivity of tested molecules is clearly observed from this figure by considering a small difference between the energy of HOMO and LUMO [81,82].



**Actives sites:** To investigate reactive sites in the tested inhibitors, molecular electrostatic potential (MESP) provides a visual method to understand the region of the electrophilic attack, nucleophilic attack and the electrostatic potential zero regions [83]. The total electron density surface mapped with molecular electrostatic potential (MEP) and contour representation of electrostatic potential of **BMQ**, **FVQ** and **STQ** are collected in Figures 13a-13b, respectively. In these maps, different values of the MESP were demonstrated with the help of different colors, which are red, yellow, green, light blue and blue. The

red and yellow colors suitable for the negative parts of the MEP are linked to electrophilic reactivity, blue colors suitable for the positive parts to the nucleophilic reactivity and the green color represents the ESP zero region. In Figures 13a-13c, the red and yellow sites are mainly observed over the benzene ring, the heteroatoms (N13, N14, and Oxygen atoms) and the conjugated double bonds, the blue and light blue sites are mainly localized around the second atom of nitrogen and benzene ring. The green regions stand for the zero electrostatic potential.

These remarks confirmed by the Mulliken charges of the inhibitor atoms as can be seen in Figure 13c [84]. As noticed that the MS acting as an electrophilic, and the nucleophilic centers are heteroatoms with free electron pairs and  $\pi$ -systems in the conjugated double bonds. The inhibitors can promote formation of a chelate on the MS surface by transferring electrons from tested molecules to Fe-atoms (d-orbital) and forming a coordinate covalent bond through the adsorption process [85].

In order to analyze the active sites of **BMQ**, **FVQ** and **STQ**, Fukui indices was used to measure the local reactivity of the inhibitors molecules and indicate their chemical reactivity for nucleophilic and electrophilic nature. The condensed Fukui functions can be computed unambiguously using a scheme of finite difference approximations such as [86]:

$$f_k^+ = P_k(N+1) - P_k(N) \quad (17)$$

$$f_k^- = P_k(N) - P_k(N-1) \quad (18)$$

where  $P_k(N+1)$ ,  $P_k(N)$ ,  $P_k(N-1)$  represent charge values of atom  $k$  for anion, neutral, and cation, respectively.

Generally, the high value of  $f_k^+$  is the preferred site for nucleophilic attack, while the sites with a high value of  $f_k^-$  are preferred for electrophilic attack. The Fukui indices for **BMQ**, **FVQ** and **STQ** are present in Tables 7-9. In **BMQ** atoms C1(0.09169), C5(0.08025), N14(0.18102), C32(0.09582), in **FVQ** atoms C1(0.08292), C15(0.10027), C22(0.09368), C26(0.10635) and in **STQ** atoms C1(0.07165), C11(0.10305), N13(0.10207), C17(0.13096), presented the highest values of  $f_k^+$  regarding the most susceptible sites for nucleophilic attacks. On the other hand, in **BMQ** atoms C12(0.1312), N14(0.11428), N15(0.09401), C32(0.0813), in **FVQ** atoms C11(0.10201), N13(0.10542), C17(0.12482), C22(0.08514) and in **STQ** atoms C1(0.07756), N13(0.06573), C15(0.09977), C26(0.06255) are the preferable sites for electrophilic attacks and consequently donating charges to the MS surface, as they presented the highest values of  $f_k^-$ . Based on these findings, the distribution of the active sites is quite different. This implies the highest capacity of adsorption of **BMQ**, **FVQ** and

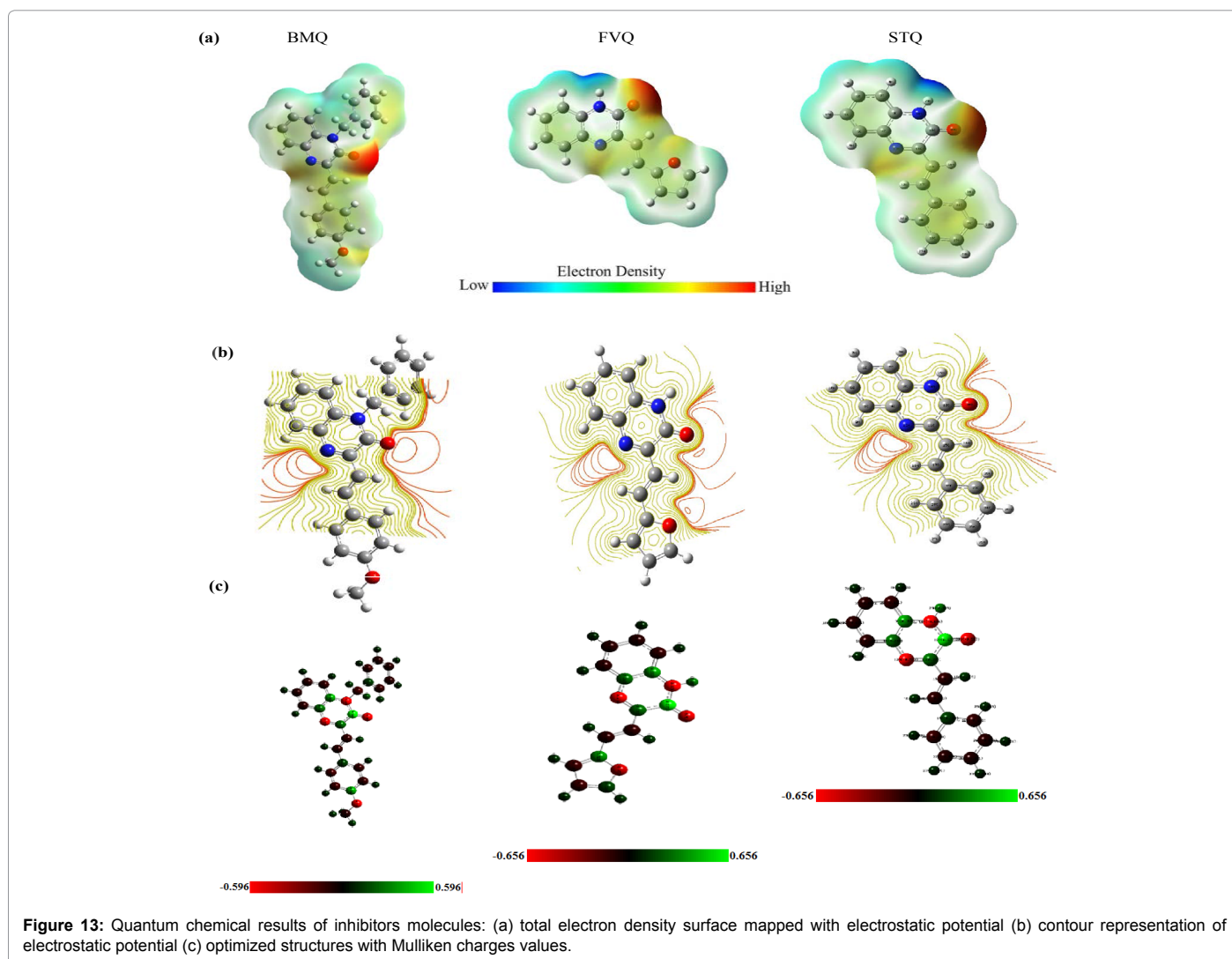


Figure 13: Quantum chemical results of inhibitors molecules: (a) total electron density surface mapped with electrostatic potential (b) contour representation of electrostatic potential (c) optimized structures with Mulliken charges values.

Atom	$P_k(N)$	$P_k(N-1)$	$P_k(N+1)$	$f_k^+$	$f_k^-$
C1	6.23558	6.18033	6.32727	0.09169	0.05525
C2	6.2817	6.25357	6.30889	0.02719	0.02813
C3	5.85758	5.84064	5.89793	0.04035	0.01694
C4	5.85067	5.83482	5.80619	-0.04448	0.01585
C5	6.23144	6.19993	6.31169	0.08025	0.03151
C6	6.2448	6.20515	6.24764	0.00284	0.03965
H7	0.76081	0.73029	0.79493	0.03412	0.03052
H8	0.7586	0.73349	0.78791	0.02931	0.02511
H9	0.75042	0.72527	0.77485	0.02443	0.02515
H10	0.75985	0.72935	0.79191	0.03206	0.0305
C11	5.87376	5.85386	5.87798	0.00422	0.0199
C12	6.04397	5.91277	6.0721	0.02813	0.1312
H13	0.76788	0.73284	0.79796	0.03008	0.03504
N14	7.48157	7.36729	7.66259	0.18102	0.11428
N15	7.36283	7.26882	7.40386	0.04103	0.09401
C16	6.26679	6.27745	6.25942	-0.00737	-0.01066
H17	0.74914	0.72348	0.76654	0.0174	0.02566
H18	0.74178	0.7262	0.7573	0.01552	0.01558
C19	6.06095	6.08532	6.04527	-0.01568	-0.02437
C20	6.23755	6.23348	6.23939	0.00184	0.00407
C21	6.22987	6.23789	6.21788	-0.01199	-0.00802
C22	6.22851	6.21531	6.23725	0.00874	0.0132
H23	0.76344	0.75466	0.76859	0.00515	0.00878
C24	6.22518	6.21622	6.23611	0.01093	0.00896
H25	0.75118	0.76433	0.74635	-0.00483	-0.01315
C26	6.23765	6.21798	6.25236	0.01471	0.01967
H27	0.75792	0.74163	0.77176	0.01384	0.01629
H28	0.75645	0.74423	0.76697	0.01052	0.01222
H29	0.75798	0.74189	0.77235	0.01437	0.01609
C30	6.24623	6.29467	6.2485	0.00227	-0.04844
H31	0.78263	0.76577	0.8019	0.01927	0.01686
C32	6.19393	6.11263	6.28975	0.09582	0.0813
H33	0.74856	0.74406	0.75768	0.00912	0.0045
C34	6.09896	6.12032	6.07953	-0.01943	-0.02136
C35	6.1919	6.16487	6.22197	0.03007	0.02703
C36	6.19907	6.18323	6.2274	0.02833	0.01584
C37	6.32432	6.31734	6.33328	0.00896	0.00698
H38	0.76043	0.75246	0.77066	0.01023	0.00797
C39	6.27355	6.26308	6.28249	0.00894	0.01047
H40	0.76582	0.76117	0.77356	0.00774	0.00465
C41	5.67758	5.63876	5.72521	0.04763	0.03882
H42	0.75837	0.74273	0.77762	0.01925	0.01564
H43	0.751	0.73485	0.77112	0.02012	0.01615
O44	8.51805	8.495	8.53246	0.01441	0.02305
C45	6.32793	6.33532	6.32191	-0.00602	-0.00739
H46	0.79377	0.78564	0.80031	0.00654	0.00813
H47	0.76826	0.7541	0.78299	0.01473	0.01416
H48	0.79378	0.7855	0.80043	0.00665	0.00828

**Table 7:** Natural population and Fukui functions of **BMQ**, calculated at B3LYP/6-31G (d, p) in gas phase.

**STQ** on the MS surface; these results are in good correlation with the experimental IE%.

### Monte Carlo (Molecular dynamic) simulation

Molecular dynamics (MD) simulation provides considerable information about the physical movements of atoms and molecules, which gives a view of the motion of the atoms after interaction at a certain time. Figure 14 represents the top and side views of the most

suitable configuration for adsorption of quinoxaline derivatives on Fe (1 1 0) substrates obtained by Monte Carlo simulation. The total energy, average total energy, van der Waals energy, electrostatic energy and intramolecular energy for **BMQ**/Fe (1 1 0) surface were calculated by optimizing the whole system; the curves are presented in Figure 15. The outputs and descriptors calculated by the Monte Carlo simulation are presented in Table 10. It is clearly observed from Figure 14 that the three quinoxaline derivatives adsorbed very nearly and in parallel to the Fe (1 1 0) surface in so as to maximize surface contact. This adsorption process occurs mainly through the formation of the insoluble film on the Fe (1 1 0) surface. It is generally noted that the adsorption process is the primary mechanism of corrosion inhibitor interaction with the MS. According to Table 10, the adsorption energies of **BMQ**, **FVQ** and **STQ** on the Fe (1 1 0) surface increased in the order **BMQ** > **FVQ** > **STQ**. The high negative values of adsorption energy of quinoxaline derivatives resulted in the strong interactions between mild steel and inhibitors molecules [87,88]. Which is in good accordance with the order of the IE% obtained by experimental and theoretical studies.

### Radial distribution function (pair correlation function)

Pair correlation function was done in order to characterize the bond length and understand the interactions of the liquid and solid materials. The pair correlation function analysis can be calculated from the trajectory output of Monte Carlo simulation, and the basic information of molecule-molecule interaction can be obtained by the calculation of bonding length. Approximately, the bond lengths of van der Waals interaction are around 5 Å ~ 10 Å, while, bond lengths around 2 Å ~ 3 Å exist for metal complexation, and H bond lengths

Atom	$P_k(N)$	$P_k(N-1)$	$P_k(N+1)$	$f_k^+$	$f_k^-$
C1	6.21617	6.13325	6.28993	0.08292	0.07376
C2	6.2738	6.27643	6.29536	-0.00263	0.02156
C3	5.83905	5.79178	5.86767	0.04727	0.02862
C4	5.88898	5.85603	5.8695	0.03295	-0.01948
C5	6.2058	6.17683	6.259	0.02897	0.0532
C6	6.25865	6.23652	6.27016	0.02213	0.01151
H7	0.75504	0.7266	0.78621	0.02844	0.03117
H8	0.75914	0.73335	0.78638	0.02579	0.02724
H9	0.74663	0.72829	0.76772	0.01834	0.02109
H10	0.75481	0.72733	0.78374	0.02748	0.02893
C11	5.84971	5.87795	5.95172	-0.02824	0.10201
C12	5.36712	5.37374	5.3666	-0.00662	-0.00052
N13	7.42909	7.36143	7.53451	0.06766	0.10542
N14	7.5928	7.56458	7.62277	0.02822	0.02997
C15	6.26023	6.15996	6.25541	0.10027	-0.00482
H16	0.73282	0.71214	0.75768	0.02068	0.02486
C17	6.21247	6.16189	6.33729	0.05058	0.12482
H18	0.74159	0.71956	0.76004	0.02203	0.01845
H19	0.56136	0.53755	0.58985	0.02381	0.02849
O20	8.61062	8.548	8.66952	0.06262	0.0589
C21	5.73382	5.70826	5.70547	0.02556	-0.02835
C22	6.28375	6.19007	6.36889	0.09368	0.08514
O23	8.44743	8.44619	8.46659	0.00124	0.01916
C24	6.33764	6.31054	6.34671	0.0271	0.00907
H25	0.74659	0.71959	0.76898	0.027	0.02239
C26	5.88059	5.77424	5.95216	0.10635	0.07157
H27	0.74606	0.71232	0.7744	0.03374	0.02834
H28	0.76826	0.73558	0.79574	0.03268	0.02748

**Table 8:** Natural population and Fukui functions of **FVQ** calculated at B3LYP/6-31G (d, p) in gas phase.

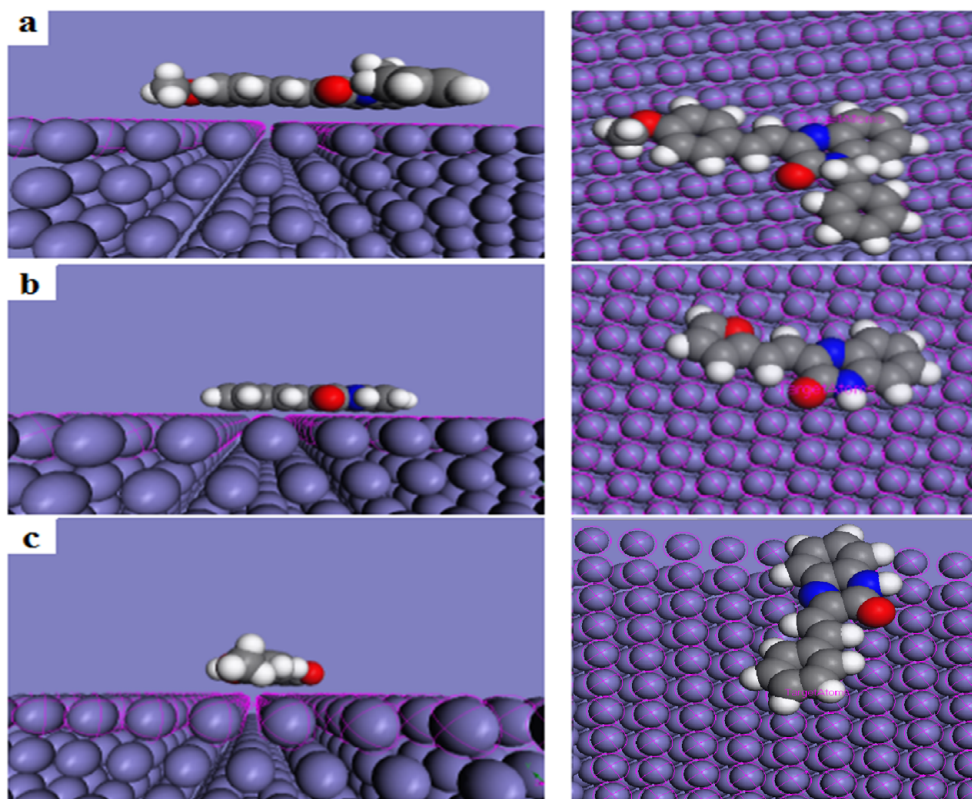


Figure 14: The side and top views of the most stable low energy configuration for the adsorption of the inhibitors on Fe (1 1 0) surface obtained through the Monte Carlo simulation. (a) BMQ, (b) FVQ, and (c) STQ.

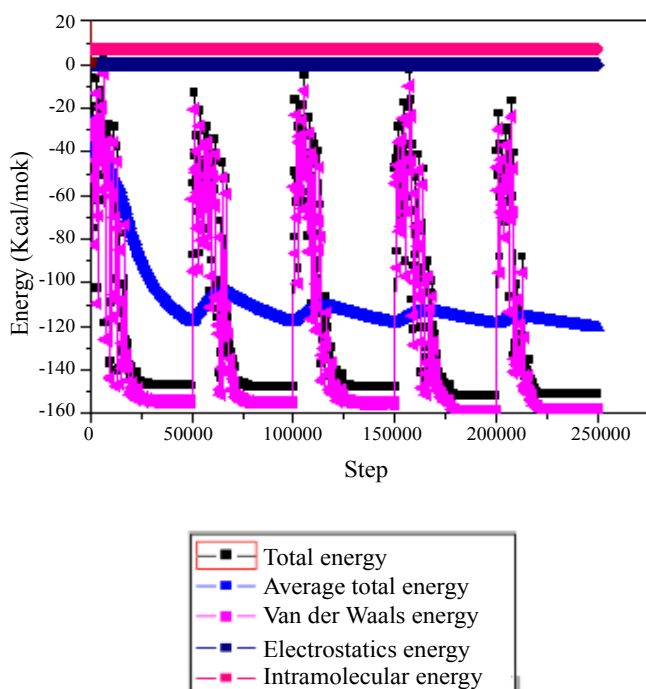


Figure 15: A typical energy profile for the adsorption progress of BMQ on Fe (110) surface using the Monte Carlo sampling procedure.

exist at around  $2 \text{ \AA} \sim 3.5 \text{ \AA}$ . The pair correlation function,  $g(r)$ , of C, N, and O of quinoxaline derivatives atoms and surface atoms was depicted in Figure 16. Generally, the chemical bonds can be formatted in correlation with the peak within  $3.5 \text{ \AA}$ , while the Van der Waals force or Coulomb force interactions are correlated with the peak outside of  $3.5 \text{ \AA}$ . We will consider the distribution of heteroatoms according to their importance on the adsorption process of chemical compounds on the metal surface, while, the carbons atoms reactivity can be obtained from  $\pi$ -system. For STQ, the highest peaks of the pair correlation function curve of O, C and N atoms appear at  $3.43 \text{ \AA}$ , and the interactive force of these atoms on the Fe (1 1 0) surface follow the same trend. For BMQ, the highest peaks of the pair correlation function curve of C, N, and O atoms appear at  $2.55 \text{ \AA}$ ,  $2.85 \text{ \AA}$ , and  $2.55 \text{ \AA}$ , respectively, and the interactive force of these atoms during the interaction with the Fe(1 1 0) surface follow the order of  $F(O) = F(C) > F(N)$ . For FVQ, the highest peaks of the pair correlation function curve of C, N, and O atoms appear at  $2.85 \text{ \AA}$ ,  $3.15 \text{ \AA}$ , and  $2.85 \text{ \AA}$ , respectively, and the interactive force of C, N, and O atoms occur during interaction with the Fe (1 1 0) surface following the order of  $F(C) = F(O) > F(N)$ . Overall, the pair correlation function curves of C, N, and O of quinoxaline derivatives and the Fe (1 1 0) surface show that the highest peak of all interaction appeared within  $3.5 \text{ \AA}$ . This indicates that chemical bonds can be formed between active centers of investigated compounds and Fe (1 1 0) atoms, confirming the high inhibition efficiency of tested inhibitors.

## Conclusion

The synthesized quinoxaline derivatives act as good corrosion inhibitors for the MS in 1.0 M HCl solution and the inhibiting performance of BMQ is better than FVQ and STQ. Polarization results

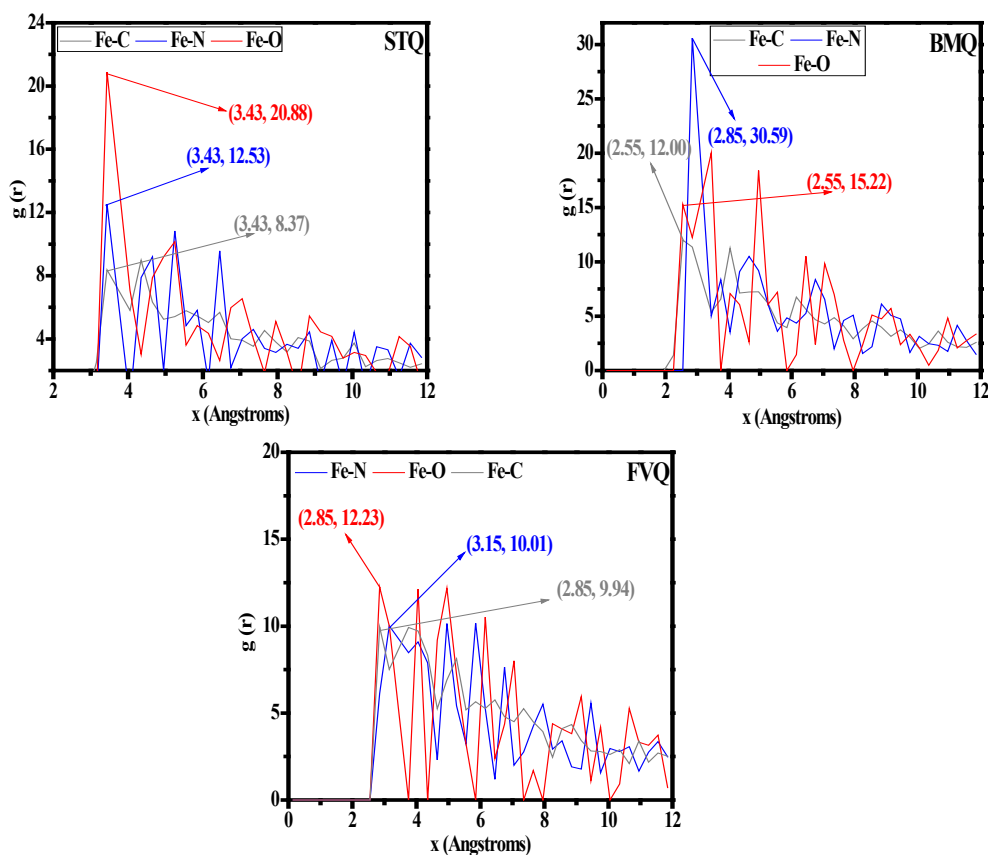


Figure 16: The pair correlation function of C, N, and O atoms from three quinoxaline derivatives with Fe atoms from Fe (1 1 0) surface.

Atom	$P_k(N)$	$P_k(N-1)$	$P_k(N+1)$	$f_k^+$	$f_k^-$
C1	6.21773	6.14017	6.28938	0.07165	0.07756
C 2	6.27371	6.27612	6.29525	0.02154	-0.00241
C 3	5.84047	5.79659	5.86754	0.02707	0.04388
C 4	5.88828	5.85992	5.86958	-0.0187	0.02836
C 5	6.20657	6.1783	6.25852	0.05195	0.02827
C 6	6.2587	6.23972	6.26991	0.01121	0.01898
H 7	0.75553	0.72885	0.7859	0.03037	0.02668
H 8	0.75969	0.73561	0.78621	0.02652	0.02408
H 9	0.74683	0.73023	0.76739	0.02056	0.0166
H 10	0.75531	0.72967	0.78345	0.02814	0.02564
C 11	5.84455	5.87515	5.9476	0.10305	-0.0306
C 12	5.36739	5.37412	5.36786	0.00047	-0.00673
N 13	7.43082	7.36509	7.53289	0.10207	0.06573
N 14	7.59265	7.56719	7.62214	0.02949	0.02546
C 15	6.2723	6.17253	6.26119	-0.01111	0.09977
H 16	0.74831	0.72985	0.77186	0.02355	0.01846
C 17	6.15179	6.1024	6.28275	0.13096	0.04939
H 18	0.7553	0.7344	0.7717	0.0164	0.0209
C 19	6.108	6.0772	6.07915	-0.02885	0.0308
C 20	6.18418	6.14051	6.22587	0.04169	0.04367
C 21	6.18885	6.16303	6.22418	0.03533	0.02582
C 22	6.32592	6.30241	6.33193	0.00601	0.02351
H 23	0.75973	0.73896	0.77395	0.01422	0.02077
C 24	6.27262	6.25183	6.28159	0.00897	0.02079

H 25	0.75621	0.7408	0.76651	0.0103	0.01541
C 26	5.66646	5.60391	5.73081	0.06435	0.06255
H 27	0.75634	0.72941	0.778	0.02166	0.02693
H 28	0.74703	0.71908	0.7698	0.02277	0.02795
H 29	0.7659	0.743	0.78435	0.01845	0.0229
O 30	8.51321	8.45657	8.53449	0.02128	0.05664
H 31	0.79209	0.77715	0.80283	0.01074	0.01494

**Table 9:** Natural population and Fukui functions of **STQ** calculated at B3LYP/6-31G (d, p) in gas phase.

.System	Total energy	Adsorption energy	Rigid adsorption energy	Deformation energy	dEad/dNi inhibitor
Fe (1 1 0)/ <b>BMQ</b>	-196.94	-204.12	-169.07	-35.05	-204.12
Fe (1 1 0)/ <b>FVQ</b>	-210.27	-203.73	-217.17	13.45	-203.73
Fe (1 1 0)/ <b>STQ</b>	-162.51	-140.20	-139.90	-0.303	-140.20

**Table 10:** Outputs and descriptors calculated by the Monte Carlo simulation for the lowest adsorption. Configurations of studied inhibitors Fe (110) surface (in kcal/mol).

showed that all tested inhibitors are of mixed type in nature. In the presence of all inhibitors, charge transfer resistance increases and double layer capacitance decreases due to adsorption of the inhibitors' molecules on the MS surface. The experimental results showed that the quinoxaline derivatives adsorb spontaneously on the MS surface and conform to the Langmuir adsorption isotherm. The adsorption process involves physical adsorption. DFT calculations, Monte Carlo simulation and RDF were performed to identify the reactivity of these molecules towards corrosion inhibition, and the results are in good agreement with the experimental investigations. Both experimental and quantum chemical results showed that the order of inhibition efficiency, for the studied compounds is as follows: **BMQ** > **FVQ** > **STQ**.

## References

- Anejjar A, Salghi R, Zarrouk A (2014) Inhibition of carbon steel corrosion in 1M HCl medium by potassium thiocyanate. *Journal of the Association of Arab Universities for Basic and Applied Sciences* 15: 21-27.
- Bammou L, Belkhaouda M, Salghi R, Benal O, Zarrouk A, et al. (2014) Corrosion inhibition of steel in sulfuric acid solution by the chenopodium ambrosioides extracts. *Journal of the Association of Arab Universities for Basic and Applied Sciences* 16: 83-90.
- Bazzi L, Salghi R, Zine E (2002) Inhibition de la corrosion de l'alliage d'aluminium 6063 au moyen de composés inorganiques dans une solution de chlorure de sodium à 3%. *Canadian Journal of Chemistry* 80: 106-112.
- Lgaz H, Benali O, Salghi R, Jodeh S, Larouj M, et al. (2016) Pyridinium derivatives as corrosion inhibitors for mild steel in 1M HCl: Electrochemical, surface and quantum chemical studies. *Der Pharma Chemica* 8: 172-190.
- Lgaz H, ELaoufir Y, Ramli Y, Oudda H (2015) Synergistic effect of potassium iodide with (E)-3-(4-methoxystyryl) quinoxalin-2 (1H)-one on the corrosion inhibition of carbon steel in 1.0 M HCl. *Der Pharma Chemica* 7: 36-45.
- Anupama KK, Ramya K, Joseph A (2016) Electrochemical and computational aspects of surface interaction and corrosion inhibition of mild steel in hydrochloric acid by *Phyllanthus amarus* leaf extract (PAE). *Journal of Molecular Liquids* 216: 146-155.
- Farag AA, Ismail AS, Migahed M (2015) Inhibition of carbon steel corrosion in acidic solution using some newly polyester derivatives. *Journal of Molecular Liquids* 211: 915-923.
- Gupta NK, Verma C, Quraishi MA, Mukherjee AK (2016) Schiff's bases derived from L-histidine and aromatic aldehydes as green corrosion inhibitors for mild steel: Experimental and theoretical studies. *Journal of Molecular Liquids* 215: 47-57.
- Murulana LC, Kabanda MM, Ebenso EE (2016) Investigation of the adsorption characteristics of some selected sulphonamide derivatives as corrosion inhibitors at mild steel/hydrochloric acid interface: Experimental, quantum chemical and QSAR studies. *Journal of Molecular Liquids* 215: 763-779.
- Ramesh Kumar S, Danaee I, Rashvand Avei M, Vijayan M (2015) Quantum chemical and experimental investigations on equipotent effects of (+) R and (-) S enantiomers of racemic amisulpride as eco-friendly corrosion inhibitors for mild steel in acidic solution. *Journal of Molecular Liquids* 212: 168-186.
- Sharma G, Raisinghani P, Abraham I, Pardasani RT, Mukherjee T (2009) Synthesis of quinoxaline quinones and regio-selectivity in their Diels-Alder cycloadditions. *Indian Journal of Chemistry (Section B)* 48: 1590-1596.
- Thomas KJR, Velusamy M, Lin JT, Chuen CH, Tao YT (2005) Chromophore-labeled quinoxaline derivatives as efficient electroluminescent materials. *Chemistry of Materials* 17: 1860-1866.
- Aguirre G, Cerecetto H, Maio DR, González M, Alfaro ME, et al. (2004) Quinoxaline N, N'-dioxide derivatives and related compounds as growth inhibitors of *Trypanosoma cruzi*. Structure-activity relationships. *Bioorganic and Medicinal Chemistry Letters* 14: 3835-3839.
- Olasunkanmi LO, Kabanda MM, Ebenso EE (2016) Quinoxaline derivatives as corrosion inhibitors for mild steel in hydrochloric acid medium: Electrochemical and quantum chemical studies. *Physica E: Low-dimensional Systems and Nanostructures* 76: 109-126.
- Obot IB, Obi-Egbedi NO, Odozi NW (2010) Acenaphtho [1, 2-b] quinoxaline as a novel corrosion inhibitor for mild steel in 0.5 M H<sub>2</sub>SO<sub>4</sub>. *Corrosion Science* 52: 923-926.
- Saranya J, Sounthari P, Parameswari K, Chitra S (2016) Acenaphtho[1,2-b]quinoxaline and acenaphtho[1,2-b]pyrazine as corrosion inhibitors for mild steel in acid medium. *Measurement* 77: 175-186.
- Obot IB, Obi-Egbedi NO (2010) 2, 3-Diphenylbenzoquinoxaline: A new corrosion inhibitor for mild steel in sulphuric acid. *Corrosion Science* 52: 282-285.
- Lashkari M, Arshadi MR (2004) DFT studies of pyridine corrosion inhibitors in electrical double layer: solvent, substrate, and electric field effects. *Chemical physics* 299: 131-137.
- Verma C, Ebenso EE, Bahadur I, Obot IB, Quraishi MA (2015) 5-(Phenylthio)-3H-pyrrole-4-carbonitriles as effective corrosion inhibitors for mild steel in 1M HCl: Experimental and theoretical investigation. *Journal of Molecular Liquids* 212: 209-218.
- Al-Mobarak N, Khaled K, Hamed MNH, Abdel-Azimb KM, Abdelshafibet NS (2010) Corrosion inhibition of copper in chloride media by 2-mercapto-4-(p-methoxyphenyl)-6-oxo-1, 6-dihydropyrimidine-5-carbonitrile: Electrochemical and theoretical study. *Arabian Journal of Chemistry* 3: 233-242.
- Yan Y, Wang X, Zhang Y, Wang P, Zhang J (2013) Theoretical evaluation of inhibition performance of purine corrosion inhibitors. *Molecular Simulation* 39: 1034-1041.
- Saha SK, Banerjee P (2015) A theoretical approach to understand the inhibition mechanism of steel corrosion with two aminobenzonitrile inhibitors. *RSC Advances* 5: 71120-71130.
- Zhang Z, Tian NC, Huang XD, Shang W, Wu L (2016) Synergistic inhibition of carbon steel corrosion in 0.5 M HCl solution by indigo carmine and some cationic organic compounds: experimental and theoretical studies. *RSC Advances* 6: 22250-22268.
- Xie SW, Liu Z, Han GC, Li W, Liu J, et al. (2015) Molecular dynamics simulation of inhibition mechanism of 3, 5-dibromo salicylaldehyde Schiff's base. *Computational and Theoretical Chemistry* 1063: 50-62.
- Lanquist J, Stacey G (1953) 568. Quinoxaline N-oxides. Part II. Oxides of Py-substituted quinoxalines. *Journal of the Chemical Society (Resumed)* pp: 2822-2830.
- Ried W, Hinsching S (1956) Synthese heterocyclisch substituierter Äthylene und Butadiene. *Justus Liebigs Annalen der Chemie* 600: 47-59.

27. Adardour K, Touir R, Ramli Y, Essassi EM (2013) Comparative inhibition study of mild steel corrosion in hydrochloric acid by new class synthesised quinoxaline derivatives: part I. *Research on Chemical Intermediates* 39: 1843-1855.
28. Ramli Y, Slimani R, Zouihri H, Lazar S, Essassi EM (2010) 2-Methyl-3-(n-octylsulfanyl)quinoxaline. *Acta Crystallographica Section E* 66: o992.
29. Lgaz H, Belkhaouda M, Larouj M, Salghi R, Jodeh S, et al. (2016) Corrosion protection of carbon steel in acidic solution by using ylang-ylang oil as green inhibitor. *Moroccan Journal of Chemistry* 4: 101-111.
30. Larouj M, Belkhaouda M, Lgaz H, Salghi R, Jodeh S, et al. (2016) Experimental and theoretical study of new synthesized organic compounds on corrosion behaviour and the inhibition of carbon steel in hydrochloric acid solution. *Der Pharma Chemica* 8: 114-133.
31. Becke AD (1992) Density-functional thermochemistry. I. The effect of the exchange-only gradient correction. *The Journal of Chemical Physics* 96: 2155-2160.
32. Becke AD (1993) Density-functional thermochemistry. III. The role of exact exchange. *The Journal of Chemical Physics* 98: 5648-5652.
33. Lee C, Yang W, Parr RG (1988) Development of the Colle-Salvetti correlation-energy formula into a functional of the electron density. *Physical Review B* 37: 785-789.
34. Frisch M, Trucks G, Schlegel H (2003) Gaussian 03, revision B. 05. Gaussian, Pittsburgh PA.
35. Materials Studio (2013) Revision 6.0. Accelrys Inc., San Diego, USA.
36. Sasikumar Y, Adekunle A, Olasunkanmi L, Bahadur I, Baskar R, et al. (2015) Experimental, quantum chemical and Monte Carlo simulation studies on the corrosion inhibition of some alkyl imidazolium ionic liquids containing tetrafluoroborate anion on mild steel in acidic medium. *Journal of Molecular Liquids* 211: 105-118.
37. Eivani AR, Zhou J, Duszczek J (2012) A new approach to incorporating the effect of nano-sized dispersoids on recrystallization inhibition into Monte Carlo simulation. *Computational Materials Science* 54: 370-377.
38. Solmaz R, Kardaş G, Çulha M, Yazıcı B, Erbil M (2008) Investigation of adsorption and inhibitive effect of 2-mercaptothiazoline on corrosion of mild steel in hydrochloric acid media. *Electrochimica Acta* 53: 5941-5952.
39. Singh DK, Kumar S, Udayabhanu G, John RP (2016) 4 (N, N-dimethylamino) benzaldehyde nicotinic hydrazone as corrosion inhibitor for mild steel in 1M HCl solution: An experimental and theoretical study. *Journal of Molecular Liquids* 216: 738-746.
40. Singh P, Srivastava V, Quraishi MA (2016) Novel quinoline derivatives as green corrosion inhibitors for mild steel in acidic medium: Electrochemical, SEM, AFM, and XPS studies. *Journal of Molecular Liquids* 216: 164-173.
41. Mourya P, Singh P, Tewari A, Rastogi RB, Singh MM, et al. (2015) Relationship between structure and inhibition behaviour of quinolinium salts for mild steel corrosion: experimental and theoretical approach. *Corrosion Science* 95: 71-87.
42. Bayol E, Gürten AA, Dursun M, Kayakirilmaz K (2008) Adsorption Behavior and inhibition corrosion effect of sodium carboxymethyl cellulose on mild steel in acidic medium. *Acta Physico-Chimica Sinica* 24: 2236-2243.
43. Avci G (2008) Inhibitor effect of N,N'-methylene diacrylamide on corrosion behavior of mild steel in 0.5 M HCl. *Materials Chemistry and Physics* 112: 234-238.
44. Yüce AO, Solmaz R, Kardaş G (2012) Investigation of inhibition effect of rhodanine-N-acetic acid on mild steel corrosion in HCl solution. *Materials Chemistry and Physics* 131: 615-620.
45. Yang Z, Zhan F, Pan Y, LYU Z, Han C, et al. (2015) Structure of a novel Benzyl Quinolium Chloride derivative and its effective corrosion inhibition in 15 wt.% hydrochloric acid. *Corrosion Science* 99: 281-294.
46. Hameed RSA (2011) Aminolysis of polyethylene terephthalate waste as corrosion inhibitor for carbon steel in HCl corrosive medium. *Advances in Applied Science Research* 2: 483-499.
47. Bentiss F, Lebrini M, Lagrenée M (2005) Thermodynamic characterization of metal dissolution and inhibitor adsorption processes in mild steel/2, 5-bis (n-thienyl)-1, 3, 4-thiadiazoles/hydrochloric acid system. *Corrosion Science* 47: 2915-2931.
48. Mu G, Li X, Liu G (2005) Synergistic inhibition between tween 60 and NaCl on the corrosion of cold rolled steel in 0.5 M sulfuric acid. *Corrosion Science* 47: 1932-1952.
49. Thomas JM, Thomas WJ, Salzberg H (1967) Introduction to the principles of heterogeneous catalysis. *Journal of The Electrochemical Society* 114: 279C-279C.
50. Odewunmi NA, Umoren SA, Gasem ZM (2015) Watermelon waste products as green corrosion inhibitors for mild steel in HCl solution. *Journal of Environmental Chemical Engineering* 3: 286-296.
51. Eddy NO, Momoh-Yahaya H, Oguzie EE (2015) Theoretical and experimental studies on the corrosion inhibition potentials of some purines for aluminum in 0.1 M HCl. *Journal of Advanced Research* 6: 203-217.
52. Zhang D, Tang Y, Qi S, Donga D, Cang H, et al. (2016) The inhibition performance of long-chain alkyl-substituted benzimidazole derivatives for corrosion of mild steel in HCl. *Corrosion Science* 102: 517-522.
53. Hussin MH, Rahim AA, Ibrahim MNM, Brosse N (2016) The capability of ultrafiltrated alkaline and organosolv oil palm (*Elaeis guineensis*) fronds lignin as green corrosion inhibitor for mild steel in 0.5 M HCl solution. *Measurement* 78: 90-103.
54. Zhang Q, Hua YX (2009) Corrosion inhibition of mild steel by alkylimidazolium ionic liquids in hydrochloric acid. *Electrochimica Acta* 54: 1881-1887.
55. Ramya K, Anupama KK, Shainy KM, Joseph A (2016) Synergistic and hydrogen bonded interaction of alkyl benzimidazoles and urea pair on mild steel in hydrochloric acid: Adsorption, electroanalytical and theoretical studies. *Journal of the Taiwan Institute of Chemical Engineers* 58: 517-527.
56. Khadiri A, Saddik R, Bekkouche K, Aounitib A, Hammouti B, et al. (2016) Gravimetric, electrochemical and quantum chemical studies of some pyridazine derivatives as corrosion inhibitors for mild steel in 1 M HCl solution. *Journal of the Taiwan Institute of Chemical Engineers* 58: 552-564.
57. Odewunmi NA, Umoren SA, Gasem ZM, Ganiyub SA, Muhammad Q (2015) L-Citrulline: An active corrosion inhibitor component of watermelon rind extract for mild steel in HCl medium. *Journal of the Taiwan Institute of Chemical Engineers* 51: 177-185.
58. Shahraki M, Dehdab M, Elmi S (2016) Theoretical studies on the corrosion inhibition performance of three amine derivatives on carbon steel: Molecular dynamics simulation and density functional theory approaches. *Journal of the Taiwan Institute of Chemical Engineers* 62: 313-321.
59. Verma CB, Quraishi M, Singh A (2015) 2-Aminobenzene-1, 3-dicarbonitriles as green corrosion inhibitor for mild steel in 1 M HCl: Electrochemical, thermodynamic, surface and quantum chemical investigation. *Journal of the Taiwan Institute of Chemical Engineers* 49: 229-239.
60. Verma C, Quraishi M, Singh A (2016) A thermodynamical, electrochemical, theoretical and surface investigation of diheteroaryl thioethers as effective corrosion inhibitors for mild steel in 1 M HCl. *Journal of the Taiwan Institute of Chemical Engineers* 58: 127-140.
61. Xu B, Gong W, Zhang K, Chen Y, et al. (2015) Theoretical prediction and experimental study of 1-Butyl-2-(4-methylphenyl)benzimidazole as a novel corrosion inhibitor for mild steel in hydrochloric acid. *Journal of the Taiwan Institute of Chemical Engineers* 51: 193-200.
62. Xu Z, Yuan S-L, Yan H, Liu C-B (2011) Adsorption of histidine and histidine-containing peptides on Au (111): a molecular dynamics study. *Colloids and Surfaces A: Physicochemical and Engineering Aspects* 380: 135-142.
63. Zhang K, Yang W, Xu B, Liua Y, Yina X, et al. (2015) Corrosion inhibition of mild steel by bromide-substituted imidazoline in hydrochloric acid. *Journal of the Taiwan Institute of Chemical Engineers* 57: 167-174.
64. Hegazy M, Abdallah M, Awad M, Rezk M (2014) Three novel di-quaternary ammonium salts as corrosion inhibitors for API X65 steel pipeline in acidic solution. Part I: experimental results. *Corrosion Science* 81: 54-64.
65. Quraishi MA (2014) 2-Amino-3, 5-dicarbonitrile-6-thio-pyridines: new and effective corrosion inhibitors for mild steel in 1 M HCl. *Industrial & Engineering Chemistry Research* 53: 2851-2859.
66. Jacob KS, Parameswaran G (2010) Corrosion inhibition of mild steel in hydrochloric acid solution by Schiff base furin thiosemicarbazone. *Corrosion Science* 52: 224-228.
67. McCafferty E (2010) Introduction to corrosion science. Springer Science & Business Media.
68. Khalil N (2003) Quantum chemical approach of corrosion inhibition. *Electrochimica Acta* 48: 2635-2640.

69. Sastri VS, Perumareddi JR (1997) Molecular orbital theoretical studies of some organic corrosion inhibitors. *Corrosion* 53: 617-622.
70. Pearson RG (1988) Absolute electronegativity and hardness: application to inorganic chemistry. *Inorganic Chemistry* 27: 734-740.
71. Martinez S (2003) Inhibitory mechanism of mimosa tannin using molecular modeling and substitutional adsorption isotherms. *Materials Chemistry and Physics* 77: 97-102.
72. Lukovits I, Kalman E, Zucchi F (2001) Corrosion inhibitors-correlation between electronic structure and efficiency. *Corrosion* 57: 3-8.
73. Rodríguez-Valdez LM, Villamizar W, Casales M (2006) Computational simulations of the molecular structure and corrosion properties of amidoethyl, aminoethyl and hydroxyethyl imidazolines inhibitors. *Corrosion Science* 48: 4053-4064.
74. Li X, Deng S, Fu H, Li T (2009) Adsorption and inhibition effect of 6-benzylaminopurine on cold rolled steel in 1.0 M HCl. *Electrochimica Acta* 54: 4089-4098.
75. Pearson RG (1988) Chemical hardness and bond dissociation energies. *Journal of the American Chemical Society* 110: 7684-7690.
76. Koch E (2005) Acid-Base interactions in energetic materials: I. the hard and soft acids and bases (HSAB) Principle—Insights to Reactivity and Sensitivity of Energetic Materials. *Propellants, Explosives, Pyrotechnics* 30: 5-16.
77. Zhou Z, Parr RG (1990) Activation hardness: new index for describing the orientation of electrophilic aromatic substitution. *Journal of the American Chemical Society* 112: 5720-5724.
78. Gece G (2008) The use of quantum chemical methods in corrosion inhibitor studies. *Corrosion Science* 50: 2981-2992.
79. Okulik N, Jubert AH (2005) Theoretical analysis of the reactive sites of non-steroidal anti-inflammatory drugs. *Internet Electronic Journal of Molecular Design* 4: 17-30.
80. Daoud D, Douadi T, Hamani H (2015) Corrosion inhibition of mild steel by two new S-heterocyclic compounds in 1 M HCl: Experimental and computational study. *Corrosion Science* 94: 21-37.
81. Tian H, Li W, Cao K, Hou B (2013) Potent inhibition of copper corrosion in neutral chloride media by novel non-toxic thiadiazole derivatives. *Corrosion Science* 73: 281-291.
82. Parr RG, Yang W (1984) Density functional approach to the frontier-electron theory of chemical reactivity. *Journal of the American Chemical Society* 106: 4049-4050.
83. Contreras RR, Fuentealba P, Galván M, Pérez P (1999) A direct evaluation of regional Fukui functions in molecules. *Chemical Physics Letters* 304: 405-413.
84. Kaya S, Kaya C, Guo L, Kandemirci F, Tüzün B, et al. (2016) Quantum chemical and molecular dynamics simulation studies on inhibition performances of some thiazole and thiadiazole derivatives against corrosion of iron. *Journal of Molecular Liquids* 219: 497-504.
85. Verma C, Olasunkanmi L O, Obot IB, Ebenso EE, Qurashi MA (2016) 5-Arylpyrimido-[4,5-b]quinoline-diones as new and sustainable corrosion inhibitors for mild steel in 1 M HCl: a combined experimental and theoretical approach. *RSC Adv* 6: 15639-15654.
86. Khaled K, El-Maghraby A (2014) Experimental, Monte Carlo and molecular dynamics simulations to investigate corrosion inhibition of mild steel in hydrochloric acid solutions. *Arabian Journal of Chemistry* 7: 319-326.
87. Kühnle A (2009) Self-assembly of organic molecules at metal surfaces. *Current Opinion in Colloid and Interface Science* 14: 157-168.
88. Shi WY, Ding C, Yan JL, Hanb XY, Lva ZM, et al. (2012) Molecular dynamics simulation for interaction of PESA and acrylic copolymers with calcite crystal surfaces. *Desalination* 291: 8-14.